

**Simulation of attitude and orbital
disturbances acting on ASPECT satellite in
the vicinity of the binary asteroid Didymos**

Erick Flores Garcia

School of Electrical Engineering

Thesis submitted for examination for the degree of Master of
Science in Technology.

Esopo December 6, 2016

Thesis supervisors:

Prof. Jaan Praks

Dr. Leonard Felicetti

Aalto University
School of Electrical Engineering

Luleå University of Technology

Thesis advisors:

M.Sc. Tuomas Tikka

M.Sc. Nemanja Jovanović

Author: Erick Flores Garcia

Title: Simulation of attitude and orbital disturbances acting on ASPECT satellite in the vicinity of the binary asteroid Didymos

Date: December 6, 2016 Language: English Number of pages: 9+84

Department of Radio Science and Engineering

Professorship: Automation Technology

Supervisor: Prof. Jaan Praks

Advisors: M.Sc. Tuomas Tikka, M.Sc. Nemanja Jovanović

Asteroid missions are gaining interest from the scientific community and many new missions are planned. The Didymos binary asteroid is a Near-Earth Object and the target of the Asteroid Impact and Deflection Assessment (AIDA). This joint mission, developed by NASA and ESA, brings the possibility to build one of the first CubeSats for deep space missions: the ASPECT satellite. Navigation systems of a deep space satellite differ greatly from the common planetary missions. Orbital environment close to an asteroid requires a case-by-case analysis. In order to develop the Attitude Determination Control System (ADCS) for the mission, one needs detailed information about orbital disturbances in the vicinity of the asteroid.

This work focuses on the development of a simulator that characterizes the orbital disturbances affecting the ASPECT satellite in the space environment near the Didymos asteroid. In this work, a model of orbital conditions and disturbances near the Didymos system was defined. The model integrates several classical and modern models of spacecraft motion and disturbance. An existing Low Earth Orbit (LEO) simulator was modified and updated accordingly to the ASPECT mission scenario. The developed simulator can be used to analyze the disturbances to be counteracted by the ADCS of the ASPECT satellite. The objective of the study was to quantify the effect of both non-gravitational and gravitational disturbances. The simulator was used to analyze different orbit scenarios related to the period of the mission and to the relative distance between the spacecraft and the asteroid system. In every scenario, the solar radiation pressure was found to be the strongest of the disturbance forces. With the developed simulator, suitable spacecraft configurations and control systems can be chosen to mitigate the effect of the disturbances on the attitude and orbit of the ASPECT satellite.

Keywords: Solar System, Small celestial bodies, CubeSat, Attitude Determination Control Systems, Orbit Disturbances

Acknowledgments

I would like to thank all the people who make possible the master programme in Space Science and Technology. I would like to give my thanks to the SpaceMaster Consortium for awarding me with the scholarship, which enabled me to fulfill this goal. Also, I would like to give my thanks to professor Jaan Praks, Tuomas Tikka, Nemanja Jovanović and the whole team involved in the development of microsatellites at Aalto University. They gave me the opportunity to work in such an interesting project and they provided me with supervision, support and guidance while developing this thesis. I would like to give special thanks to my family who has always been my greatest support and motivation to pursue my dreams. Many thanks to all the SpaceMaster community for sharing this amazing experience. In essence, I want to thank every single person that shared time, knowledge and experience with me during this journey. This adventure opened my eyes and mind to a new and amazing way of perceiving life.

Otaniemi, December 6, 2016

Erick Flores Garcia

Contents

Abstract	ii
Acknowledgments	iii
Contents	iv
Symbols and Abbreviations	viii
1 Introduction	1
1.1 Exploration of the Didymos Asteroid	1
1.2 Modelling and Simulation of a Binary Asteroid Environment	2
1.3 Thesis Structure Overview	3
2 Small Body Exploration Missions	5
2.1 Motivations of Small Body Exploration	6
2.2 Space Missions to Comets and Asteroids	7
2.2.1 Asteroid Exploration	8
2.2.2 Comet Exploration	10
2.3 Deep Space Missions GNC Systems	12
3 AIDA and ASPECT Missions	14
3.1 Details and Requirements of the ASPECT Mission.	16
4 Theory of Small Bodies: Asteroid Systems	22
4.1 Modelling Small Body Environments	22
4.1.1 Mass and Density	22
4.1.2 Spin State	23
4.1.3 Shape and Morphology	24
4.1.4 Gravitational Potential: Spherical Harmonics Model	24
4.2 Dynamical and Physical Properties of Didymos	27
5 Modelling of a Spacecraft Orbiting a Binary Asteroid System	31
5.1 Coordinate Systems	31
5.1.1 Coordinate System Transformations	34
5.2 Ephemerides	35
5.3 Disturbances Acting on the Spacecraft	35
5.4 Disturbance Modelling	37
5.4.1 Gravitational Disturbances	37
5.4.2 Solar Radiation Pressure	40
5.4.3 Total Disturbance Torque	41
5.5 Orbit Propagator	41
5.6 Satellite Model	43

6 Simulation Environment	45
6.1 Simulation Framework	45
6.2 Ephemerides Models	47
6.3 Dynamic and Kinematic Models	48
6.3.1 Orbit Propagator	48
6.3.2 Spacecraft Attitude	50
6.4 Environment Disturbances	50
6.4.1 Third Body Perturbation	51
6.4.2 Gravity Gradient Model	52
6.4.3 Asteroid Zonal Harmonics	53
6.4.4 Solar Radiation Model	54
6.5 Masks: Constants and Parameters	56
7 Simulator Testing and Functional Verification	58
7.1 Simulation Exemplification	58
7.2 Demonstration Cases	61
7.3 Solar Absorption Coefficient	67
8 Summary of Findings	69
8.1 Further Work	69
References	71
A Quaternions	76
B Legendre Polynomials	78
C Simulation set-up	79

List of Figures

1 The inner Solar System and its asteroids, from the Sun to Jupiter	6
2 Asteroids and comets imaged by spacecraft	9
3 Comparison image of the nuclei of comets Tempel 1 and Hartley 2	11
4 Comet Churyumov-Gerasimenko and Rosetta's final destination	12
5 AIDA mission concept infographic	15
6 AIDA mission goals	16
7 ASPECT platform concepts	17
8 Representation of the operation orbit of the spacecraft	19
9 Top view of the orbit plane	19
10 Didymos ephemeris and critical distances during the mission	20
11 Distances from spacecraft to the Earth, the Sun and the asteroid	21
12 Mass distribution geometry	25
13 The triaxial ellipsoid	26
14 Preliminary shape model of the Didymos system	29

15	Asteroid inertial reference frame	32
16	Spacecraft reference frame	33
17	Representation of the orbit reference frame	33
18	Controller reference frame	34
19	Illustration of the gravity gradient torque	40
20	Circular restricted three body problem	42
21	SIMULINK implementation of the asteroid space environment	46
22	SIMULINK implementation of the simulation time	47
23	SIMULINK implementation of the ephemeris model	48
24	SIMULINK implementation of the orbit propagator	49
25	SIMULINK implementation of dynamics and kinematics of the satellite	50
26	SIMULINK implementation of the third body disturbance with Earth as the perturbing body	52
27	SIMULINK implementation of the gravity gradient disturbance	53
28	SIMULINK implementation of the asteroid zonal harmonics model	54
29	SIMULINK implementation of the solar radiation pressure model	55
30	Magnitude of the disturbance torques produced by the different sources. Part 1	59
30	Magnitude of the disturbance torques produced by the different sources. Part 2	60
31	Maximum and minimum distances between the Sun and the Didymos system	62
32	Didymos trajectory end of September 2022	63
33	Didymos trajectory middle of April 2023	64
34	ASPECT satellite orbit motion in the asteroid fixed reference frame at different radii	65
35	Solar Radiation Pressure torque magnitude acting on the ASPECT satellite	67
C1	Selecting the dates of interest to load the ephemeris of the Didymos	79
C2	Trajectory of the Didymos asteroid during the mission	80
C3	Example of a partial trajectory of the Didymos asteroid	81
C4	Principal layer of the SIMULINK simulator	82
C5	SIMULINK model masks containing the adjustable parameters of the simulation	83
C6	Output variables in the workspace of the Matlab environment	84

List of Tables

1	Basic platform characteristics required in the ADCS design	17
2	Didymos system basic properties	27
3	Didymos orbital elements and mutual orbit properties	28
4	External disturbances that affect a spacecraft	36
5	Mask parameters and constants used in the simulator	57
6	Environment disturbances at 1 AU from the Sun	66

7	Environment disturbances at 1.8 AU from the Sun	66
---	---	----

Symbols and Abbreviations

Greek symbols

δ	density
θ	latitude
λ	longitude
μ_p	gravitational constant of body p
ρ	position vector of differential mass
σ	local density
ω	angular speed

Roman symbols

A	cross-sectional area perpendicular to the vector that joins the spacecraft to the Sun
a	semi-major axis
C_{nm}	spherical harmonic coefficient of degree n and order m
G	gravitational constant
h	angular momentum
I	moment of inertia
K	solar absorption coefficient
M	body mass
${}^S N_{AZH}$	non-spherical shape torque disturbance
${}^S N_{ext}$	total torque disturbance
${}^S N_{GG}$	gravity gradient torque disturbance
${}^S N_{TBP}$	third body torque disturbance
${}^S N_R$	solar radiation pressure torque disturbance
P_{nm}	Legendre polynomial of degree n and order m
R	mean radius
\mathbf{R}_p	perturbing acceleration due to body p
${}^S R_a$	position vector of body a in the s frame
T	orbit period
U	gravitational potential
V	volume

Operators

a	boldface indicates vector
\hat{a}	normalized/unit vector
∇	differential operator
$\frac{d^m}{du^m}$	derivative of order m with respect to u
$ \mathbf{a} $	norm/magnitude of vector a
$\sum_{i=0}^n$	sum over index $i = 1 \dots n$
$\mathbf{a} \cdot \mathbf{b}$	dot product of vector a and b
$\mathbf{a} \times \mathbf{b}$	cross product of vector a and b
\dot{a}	time derivative of a
floor	largest previous integer

Abbreviations

ADCS	Attitude Determination and Control System
AIDA	Asteroid Impact and Deflection Assessment
AIM	Asteroid Impact Mission
ASPECT	Asteroid Spectral Imaging Mission
COPINS	Cubesat Opportunity Payloads
DART	Double Asteroid Redirection Test
DLR	German Aerospace Center
ESA	European Space Agency
GNC	Guidance, Navigation and Control
ICE	International Cometary Explorer
JAXA	Japan Aerospace Exploration Agency
JHUAPL	Johns Hopkins University Applied Physics Laboratory
JPL	Jet Propulsion Laboratory
LEO	Low Earth Orbit
MASCOT	Mobile Asteroid Surface Scout
MONTE	Mission-Analyses Operations Navigation Toolkit Environment
NASA	National Aeronautics and Space Administration
NEO	Near-Earth Object
NEAR	Near-Earth Asteroid Rendezvous
VTT	Technical Research Centre of Finland
YORP	Yarkovsky-O'Keefe-Radzievskii-Paddack

1 Introduction

Exploration of Solar System small bodies, such as asteroids, comets and planetary satellites, is an interesting endeavor at the forefront of planetary science. These bodies provide information about the past of the Solar System. The asteroids reveal the evolution of the planetary formation and the comets provide information about the chemical composition of the proto-planetary satellites before the formation of the modern Solar System. Other motives besides science are the identification (and potential exploitation) of extra-terrestrial resources and the mitigation of hazardous asteroids and comets that may have impact trajectories with the Earth. In order to observe these bodies, nearly 20 space missions have been performed. Each of them has contributed to science and technology development. Anteriorly, it was thought, that asteroids were monolithic bodies with no regolith material on their surface. However, new high-resolution imaging techniques have shown that they are actually covered with boulders, pebbles and rocks. Hence, changing the expected scenario for the potential extraction of materials. Similarly, when the Rosetta spacecraft tested a new mass spectroscopy technique, organic molecules were discovered in the comet Churyumov-Gerasimenko, unlocking part of the enigma behind the beginning of life. [1, 2] [2]

1.1 Exploration of the Didymos Asteroid

In a joint effort campaign, several space agencies across the world are developing a mission called Asteroid Impact and Deflection Assessment (AIDA). This mission is planned to be ready for launch in 2020. The project consists of two independent missions, whose common target is the binary asteroid system (65803) Didymos (1996 GT). A binary asteroid is composed by two bodies attached to each other by their gravitational fields. Usually, one body is considerably more massive than the other; this one is referred as the primary, whereas the smaller one is designated as the secondary [1]. The first mission, the NASA Double Asteroid Redirection Test (DART), is an asteroid impactor, which would crash into the secondary, changing the orbital period of the latter respect to the primary. The second one, the ESA Asteroid Impact Mission (AIM), is an asteroid rendezvous spacecraft which would observe the changes in the system caused by the impactor. The main objectives of this mission are to characterise the dynamic state of the system and to study how the physical properties of the asteroid can be inferred based on the observations [3]. [3]

In addition to the main spacecraft, the AIM mission will also include a lander and two or more CubeSats, which will be released in the Didymos system. A CubeSat is a miniaturized satellite composed by cubic units of 10 cm per side [4]. This arrangement opens the possibility for secondary scientific payloads. The Asteroid Spectral Imaging Mission (ASPECT) is a CubeSat satellite proposal by VTT, Aalto University and the University of Helsinki. The objective of this mission is to study the composition of the Didymos binary asteroid and to analyse the effects of space weathering and shock metamorphism in order to gain knowledge about the formation

and evolution of the Solar System. [5]

1.2 Modelling and Simulation of a Binary Asteroid Environment

Testing prototypes in realistic scenarios is not always viable or it can be extremely costly. The alternative is to perform simulations. In particular, designing a spacecraft and space missions relies heavily on numerical simulations. Simulations allow better designing, prototyping and validation methods of a satellite before it is produced [6, 7]. Further, achieving interplanetary flights requires breakthroughs in several fields such as: mechanical engineering, astrodynamics, telecommunications and digital computer systems [8, 9]. The ASPECT satellite requires a specific attitude accuracy and orbit stability to successfully complete its objective. A preliminary study and design process must be done considering the relationship between all the disturbances of the space environment and the spacecraft. The main objective of this thesis consists of providing a simulation environment of the disturbances associated to a spacecraft orbiting the Didymos asteroid system. This simulator can be used to analyse and develop the Attitude Determination Dontrol System (ADCS) of the ASPECT satellite.

The first step of this project is to fully understand and to model the environment of the Didymos system. The model should integrate several classical and modern models of spacecraft motion and disturbance. Each asteroid environment presents unique properties and conditions. Therefore, each mission is examined in a case-by-case manner. Further, due to the novelty of the topic, much of the information is documented in several research papers. However, it is possible to establish a base for modelling by revising the development of prior similar missions to small celestial bodies. For instance, the observation of asteroid Eros and Toutatis helped to develop improved models of uniform and complex rotators. [1] Similarly, the analysis of other asteroids such as Vespa, Gaspra and Castelia, has contributed to model the attitude dynamics and stability of spacecraft in the vicinity of irregular bodies [10]. Likewise, Asteroid KW4 served as a motivating model of a binary system [1, 11]. Another aspect to notice is that normally asteroid orbiters tend to be affected differently by non-gravitational disturbances. Unlike with Earth orbiters, the solar radiation pressure and solar tide effects become the strongest sources of disturbance. Concisely, the Didymos asteroid requires an adaptation and integration of these models in order to be fully described. The comprehensive text by D.J. Scheeres [1] covers the complete up-to-date analysis techniques to describe spacecraft motion in strongly perturbed environments. [1]

Further, the main contribution of this thesis consists in implementing the models into a software platform that can be used for the ADCS design and analysis. Mission design and navigation simulations demand a large set of analysis techniques and software tools at different levels. The rigor of a real deep space mission obliges the usage of the latest generation of navigation software. For example, the Mission-Analysis Operations Navigation Toolkit Environment by NASA (MONTE), a software package by the Jet Propulsion Laboratory of NASA (JPL), includes all of the features

demanded in a project such as the AIDA mission. The MONTE software can perform orbit propagation, orbit optimization, maneuvering, observational filtering, spacecraft guidance and attitude control for deep space missions. In addition, it is structured using Object-oriented programming, easing its maintenance and increasing its extensibility. On the contrary, license management and commercialism of the product limit its availability during the current state of the ASPECT project. Other alternatives exist as well and can be found in [12]. Nevertheless, they endure equivalent limitations. Overall, a software that implements and integrates a microsatellite deep space mission to a unique target asteroid is not easily and/or freely available. Therefore, the necessity and importance of a software tool that can be used for the development of the ASPECT mission. [9, 13]

For the precedent reasons, an available Low Earth Orbit (LEO) simulator [4] was modified and updated accordingly to the ASPECT mission scenario. The Department of Control Engineering in Aalborg University developed a simulator in order to design and build the AAUSAT-II satellite. This spacecraft is a CubeSat built with education purposes. The Aalborg simulator contemplates only LEO missions, which have distinct operation conditions and disturbances compared to an asteroid system. However, the simulator presents a generic architecture platform that integrates independent subsystems. Such architecture permits changes in a subsystem without having a direct effect on the rest. In this manner, any modification, upgrading, testing or verification turns out to be fairly simple. This simulator was configured and reprogrammed according to the models of a binary asteroid system. [1, 4]

1.3 Thesis Structure Overview

This document follows a specific structure. Firstly, the history of small body exploration missions along with its principal motives is given in section 2. It also covers navigation systems utilised in small celestial bodies missions. Secondly, the AIDA, the AIM, and most importantly, the ASPECT mission details and requirements are explained in section 3. The purpose is to establish a starting point and a base for this project. Thirdly, section 4 introduces the theory of small bodies in the Solar System, their orbits, sizes, properties and the forces due to the environment surrounding them. These features are important to portray the mechanics of an asteroid system [1]. Accordingly, suitable models can be chosen. In addition, this chapter presents the latest information up to date of the Didymos asteroid with the purpose of linking its properties to the previously defined concepts given in the theory. Next, section 5 defines the mathematical models that govern the dynamics and kinematics of a satellite in the proximity of the binary asteroid with the main sources of disturbance. Thereafter, the Matlab and SIMULINK implementation of the models is presented in section 6. Here, each subsystem is individually described with its corresponding input and output variables; as well as the constant parameters that characterise the simulation. The tests and functional verification are detailed in section 7. The results portray the disturbance analysis of different simulation setups regarding the configuration of the spacecraft and the asteroid environment. Finally, in section 8,

a summary of the findings and the insights of the simulator are given. In addition, it includes some suggestions for future research regarding the development of the ADCS of the ASPECT satellite.

2 Small Body Exploration Missions

This chapter provides a review and insights of small body exploration missions. It includes an overview of the motivations and the history of the most relevant missions concerning comets and asteroids. Finally, it includes a description of Guidance, Navigation and Control Systems used in some of these missions.

Near-Earth Objects (NEOs) are a collection of comets and asteroids that have entered the Earth's gravitational neighbourhood. Comets, composed mainly of ice mixed with dust particles, originated in the cold outer planetary system. The rocky asteroids were formed in the inner solar system in between the orbits of Mars and Jupiter. The Figure 1 depicts a representation of the distribution of these bodies in the solar system. [1]

These bodies are of scientific interest, because they provide details about the formation of the solar system which occurred some 4.6 billions years ago. They represent the residual pieces from the process that formed the inner planets: Mercury, Venus, Earth and Mars. Second, they represent a significant changing factor on the Earth's biosphere and geology with its continuous collisions. Thirdly, they offer a source of volatile and rich supply of resources that could be exploited for the exploration of the solar system. [14]

Additionally, small bodies, especially Near-Earth asteroids, have become of interest for human exploration because these objects can be easily approached from our planet. Moreover, the challenge of the design and development of spacecraft capable of performing this type of missions improves technology significantly. For this reason, and specially in recent years, space missions targeting small bodies have been developed. The Giotto mission to Comet Halley (1985) and the recent Rosetta mission (2004) to Comet Churyumov-Gerasimenko, both developed by ESA, are two good examples of missions which improved our understanding of the Solar System as well as promoted the progress of technology. [11, 15]

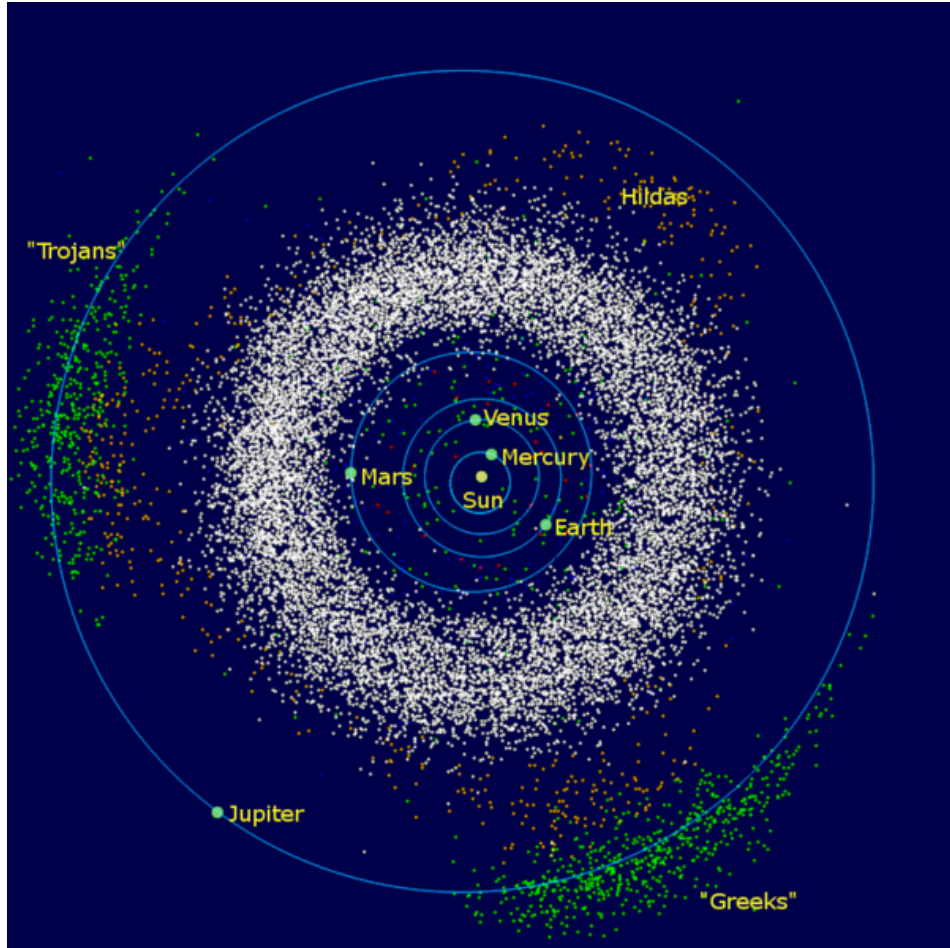


Figure 1: The inner Solar System, from the Sun to Jupiter. It includes the asteroid belt (the white cloud), the Hildas (the orange "triangle" just inside the orbit of Jupiter), the Jupiter trojans (green), and the near-Earth asteroids. The group that leads Jupiter are called the "Greeks" and the trailing group are called the "Trojans" [16].

2.1 Motivations of Small Body Exploration

The first and elemental motivation to explore small bodies is probably the innate scientific curiosity of the human kind. Numerous theories have been pronounced about the source and nature of bodies that compose the solar system. Comets and asteroids are considered remnants of the early stages of our planetary system. These bodies present similar, but also unique characteristics compared to each other and analysing them permits us to broaden our knowledge about the Solar System. Thus, space missions targeting these bodies become of high importance. However, the

observation of these bodies carries technological challenges. If these challenges are overcome, then more accurate conclusions can be made about the evolution of our planetary system. Small bodies have considerable differences compared to planets, such as the strength of its gravitational field or the strength of the disturbances coming from non-gravitational sources that sometimes tend to be neglected in planetary exploration missions. [17, 1]

In addition, the development of technology is also compromised due to the rising costs of various scarce elements, which are used to produce key components in technology; for instance, computer chips or aerospace circuitry. Many of these elements (gold, iron, manganese, platinum, rhodium, tungsten, among others) were deposited on the Earth by meteor impacts. [18] However, they will not last forever and in the future, space resources can become competitive with Earth resources. On the other hand, there are future missions with the objective of colonising the Solar System, e.g. sending people to Mars or the Moon. Therefore, it would be essential to find and exploit the resources found in the space environment. Engineers and scientists would need to find suitable manners to obtain materials from asteroids for different purposes like construction or to produce propellant for spacecrafts. [11] Asteroid mining could provide practically unlimited resources. Although, before going into this venture; a survey from an economic and feasibility perspective should be done. Currently, there are some companies, such as Deep Space Industries, with the objective of performing asteroid mining, inspiring new research and projects that would push forward our current limits of technology. [19, 11]

Another motive is the protection of the Earth from the impact of small bodies. The idea of planetary defence arose first as part of the fiction; however, during the 20th century it turned into a more serious theme, when strong evidence about huge effects of their incoming impacts. Evidence suggests that a big meteor impact occurred 65 million years ago on the surface of the Earth and that it had a catastrophic effect on the biosphere. For this reason, meteorites are considered a big potential threat to life. [17]

The first attempts to define the requirements for these protection missions were done by institutions in the USA. Besides, more accurate estimations about the orbits of these small bodies were possible with the development of better observation instruments and computers. In 1994, a comet hit Jupiter and the impact was observed by the Hubble space telescope and the effects were then measured by Galileo, Ulysses and Voyager spacecraft. The whole event made clearer the fact that something should be done regarding small bodies deflection and since then, wide research has been encouraged and several deflection methods have been presented in the literature. The joint mission Asteroid Impact & Deflection Assessment is a perfect example. [17, 20]

2.2 Space Missions to Comets and Asteroids

In this section a brief review of the observation methods and space missions targeting asteroids and comets is presented. Two types of these missions are defined: flyby and rendezvous missions. Flyby missions provide more limited information, because the

spacecrafts in these missions do not spend as much time near the small celestial body as they would do in a rendezvous mission. Until today, 12 spacecraft have visited or are being planned to visit and to observe a total of 12 asteroids and 7 comets. [11]

2.2.1 Asteroid Exploration

Optical observations are used as the primary method to discover asteroids. Asteroid Ceres was the first of these bodies to be acknowledged back in 1801. Nowadays, the discovery rate has increased, allowing surveys for Near-Earth asteroids. Currently, the number ascends up to 300,000 in the Main Belt. Although, we only know precise orbits of half of them. [1, 11] These observations detect asteroids as points of light, but with new optical technologies on Earth and in orbit, asteroids can be imaged and a few physical properties can be deduced from these observations. The body size can be estimated depending on the brightness observed. The shape of an asteroid and its spin period can be constrained depending on the fluctuation of the reflected light. If there are abrupt changes on it, probably a binary system is observed. Observations at different wavelengths also reveal the composition and temperature of the asteroid. There are other observation methodologies such as radar observations. For example, the Range Doppler radar which allows a better derivation of the orbit, the shape, and the spin state of an asteroid. These observation techniques have allowed accurate imaging of the bodies just as shown in Figure 2. This is important because kinematic and dynamic models of the body can be estimated. These are necessary for the disturbance calculation of a spacecraft orbiting it. [1]

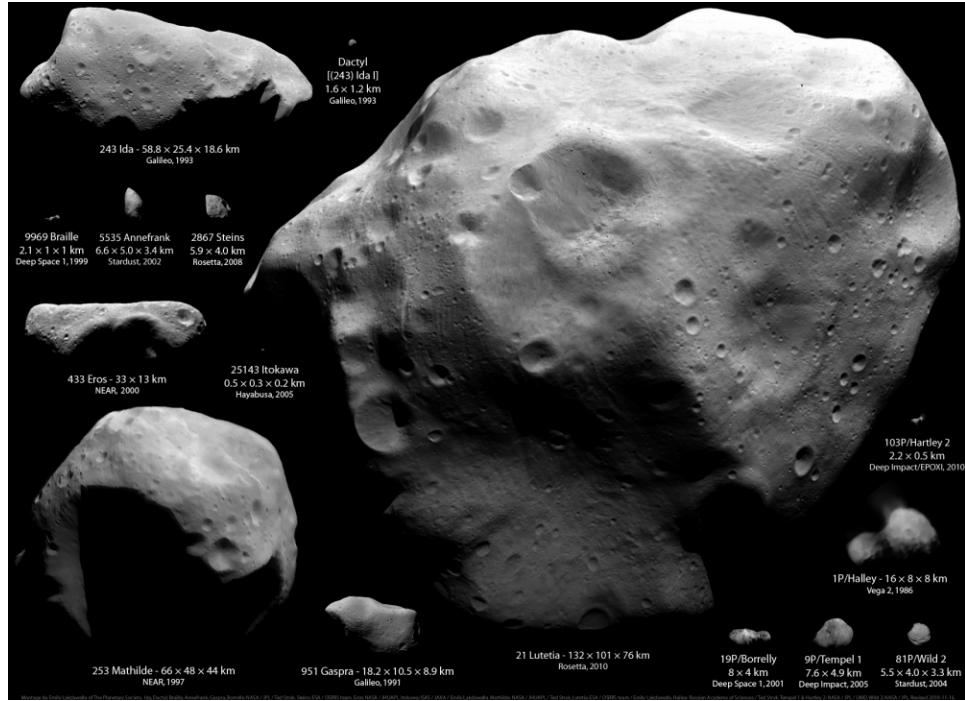


Figure 2: Compilation of asteroids and comets imaged by spacecraft. Ida, Dactyl, Braille, Annegrank, Gaspra, Borrelly: NASA/JPL/Ted Stryk. Steins: ESA/OSIRIS team. Eros: NASA/JHUAPL. Itokawa: ISAS/JAXA/Emily Lakdawalla. Mathilde: NASA/JHUAPL/Ted Stryk. Lutetia: ESA/OSIRIS team/Emily Lakdawalla. Halley: Russian Academy of Sciences/Ted Stryk. Tempel 1: NASA/JPL/UMD. Wild 2: NASA/JPL. [1].

One of the first relevant mission regarding asteroids was the Galileo mission. It was developed to observe the orbit of Jupiter, nonetheless during its journey, its objective was extended to make a flyby of the asteroids Ida and Gaspra. The flyby revealed that the former was a binary system; the first one ever observed. Thereafter in 1996, the Near-Earth Asteroid Rendezvous (NEAR) spacecraft was launched and made successful flybys of asteroids Mathilde and Eros. This mission was the first attempt to land on an asteroid. The objective was to comprehend its composition, morphology, magnetic field and mass distribution among other physical properties. The interaction between the solar wind and the asteroid surface was analysed as well. However, the scheduled rendezvous main engine failed, thus permitting only a flyby. Then in 1999, a mission called DeepSpace-1 (by NASA) targeted the asteroid Braille with the purpose of testing new instruments that permitted to perform the first imaging of an asteroid. [1, 11, 21]

Further, the Japan Aerospace Exploration Agency (JAXA) developed the mission Hayabusa and launched an unmanned spacecraft in 2003 with the purpose of returning a sample material from the small NEO asteroid Itokawa to Earth. The rendezvous

occurred in November 2005 and the samples were returned in June of 2010. The samples provided insights about the shape of the asteroid, the spin, the topography, the composition, the density and its colour. [11, 22]

Afterwards and currently operating, a successor asteroid explorer Hayabusa2 was designed again by JAXA. The target is the asteroid Ryugu, a C-type asteroid, which means that it is carbonaceous body and generally of higher interest because it is considered to contain more organic minerals. The objective is to clarify the origin of life and the interaction between organic matter and water in the solar system by analysing return samples. [23]

Similarly, two more rendezvous missions are planned to be launched in 2016 and in 2020. First, the OSIRIS-REx mission, which will travel to the near-Earth asteroid Bennu and would bring a sample back to Earth in 2023 [24]. Second, the AIDA mission, the main topic that serves as the primary motivation and base of this thesis. As stated in the introduction, this joint NASA-ESA mission is planned to meet the binary asteroid Didymos in order to observe the effects of a direct impact on its surface, therefore providing insights about its composition and about methods for asteroid deflection. A full section in this chapter is dedicated in the next pages to describe the details of this mission. [25]

2.2.2 Comet Exploration

This subsection provides information about the missions targeting the study of comets. Even though this thesis focuses into the analysis of an asteroid system, it is still relevant to mention the scientific and technological contributions of missions targeting comets. The observation of comets predates the observation of asteroids considering that they are visible for the naked-eye and simple telescopic observations. Nonetheless, they have lagged behind in rendezvous missions, since only one mission, the Rosetta mission, has been accomplished. Optical and radar techniques are used to determine the physical properties that comets posses. [1]

The International Cometary Explorer (ICE) was launched on 12 August 1978 by NASA. Its main objective was to analyse the interaction between the solar wind and the Earth's magnetosphere. However, after completing its main mission, the spacecraft was reactivated and diverted to pass within approximately 7,860 kilometers from the comet Giacobini-Zinner in 1985. Second, Vega-1 and Vega-2 were two Russian probes that were sent to Venus, but they also passed and photographed Comet Halley at distances over 8,000 kilometers in 1986. [2] This comet became the first one to be the main target of an exploration mission. Launched in 1985, the Giotto spacecraft was a flyby collaborative mission developed by ESA (its first deep space mission), NASA, the former USSR and Japan. The flyby mission passed at a distance of 600 km from the comet, but the information obtained was not sufficient to make a full description of the system; however, the shape, composition and the rotation state of the comet were determined. Furthermore, the same spacecraft was reactivated in 1992 to flyby the Comet Grigg-Skjellerup [26]. [1, 2, 11]

Following these observations, the next significant comet mission was done by the DeepSpace 1 spacecraft in 2001, when it visited the comet Borrelly. It approached

within 26 km and revealed that the comet shape could be greatly bifurcated. Thereafter in 2004, the comet Wild 2 was the target of the spacecraft Stardust. It became the first spacecraft that returned a sample from a comet's coma, revealing a different surface morphology compared to the previous comet. [2, 11, 1]

Next, in 2005, the Deep Impact spacecraft was designed to determine the strength of a cometary surface. This was done by sending a 370-kg impactor onto the surface of comet Tempel 1 to create a crater. However, unforeseen high dust level and high density of the dust after the impact obstructed the imaging of the crater. Still, this mission provided the highest-resolution image of the surface of the comet up to that date, which helped to understand more about the nature of these bodies. This mission was complemented afterwards in 2011, when the Stardust spacecraft could identify and image (with a low resolution) the crater made by the impactor. In November of 2010, the same spacecraft, the Deep Impact, performed a flyby of comet Hartley 2 and imaged the body exposing the presence of snow orbiting the comet. Figure 3 shows the images obtained of comet Tempel 1 and comet Hartley 2. [1, 11]

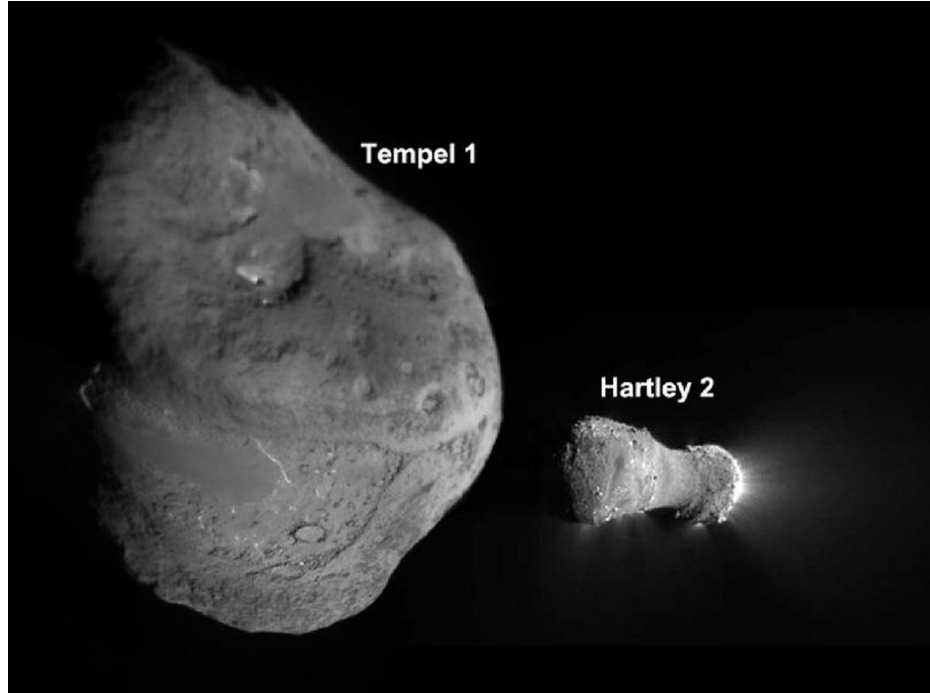


Figure 3: Comparison image of the nuclei of comets Tempel 1 and Hartley 2 [1].

The Rosetta mission is probably the most successful and popular exploration mission that has been done. Since launched on 2 March 2004, it has passed two asteroids: Setins in 2008 and Lutetia in 2010. However, its main mission was reaching and studying in detail the comet Churyumov-Gerasimenko in 2014. After a series of maneuvers, this space probe, was captured in the orbit of the comet followed

by the release of Philae, its lander module, on the surface of the small body. The probe discovered a magnetic field, which might be caused by the solar wind rather than being a intrinsic characteristic of the comet. It also analysed the composition of the water vapour, as well as the mechanisms that degrade water and carbon dioxide, releasing them from the nucleus into its coma. Figure 4 shows the comet Churyumov-Gerasimenko and the target region where the spacecraft landed; this region was chosen due to the scientific potential and because of operational restraints, involved in the landing process. [11, 2]



Figure 4: Comet Churyumov-Gerasimenko and Rosetta’s final destination (red circle) [2].

2.3 Deep Space Missions GNC Systems

A deep space mission involves visiting other natural celestial bodies in the Solar System. One of the major challenges of deep space missions consists of determining the guidance, navigation and control system (GNC system). GNC consists of determining the orbit and attitude of a spacecraft at any time, as well as the control of both aspects. [27] This implies that ADCS is an element of the GNC system. To execute its functions, GNC utilises sensors and control devices. The former ones are used to determine the position, orientation and velocity state of the spacecraft. The latter ones change the pointing direction, the rate of turning and the speed of the spacecraft. Examples of sensors include sun sensors, star trackers and inertial measuring units. Whereas control devices, in deep space missions, can be reaction control system thrusters or reaction wheels. [28]

Existing GNC techniques include Earth based radiometric tracking data and on-board optical data. An inherent inconvenience is the time that takes to make a round trip of the radio signal between the Earth and the spacecraft. For this reason,

maneuvers can take from hours to several days to be commanded and performed. The evident way to overcome this issue is by performing the navigation functions on-board the spacecraft. AutoNav by NASA is an example of such system. It has been successfully implemented on five missions: Deep Space 1, Stardust, Deep Impact, EPOXI and Stardust NExT. However, future missions are tightening the design and performance requirements. [27]

Spacecraft are now demanded to respond autonomously to new environments including solar wind, comet outgassing and high radiation. The GNC systems need simulations during the design phase and during the analysis phase of real-time data. Both phases require a large set of software tools. These tools must consider different levels of precision and fidelity. The software serves to propagate and optimize trajectories; to reduce observational quantities; and to simulate guidance, maneuvering and attitude control of a spacecraft. [27, 9]

An example, capable of supporting initial studies, is called MONTE. Developed in the NASA's Jet Propulsion Laboratory, this software is at the forefront of deep space navigation technologies. Unfortunately, its licensing and selected availability makes it difficult to procure. [9] Another example of software with similar capabilities is the Spacecraft Control Toolbox by Princeton Satellite Systems Inc. Nevertheless, its procurement is equally conditioned [7]. Therefore, the importance of the development of the simulator in this thesis. The simulator permits a trustworthy estimation for the early design phase.

3 AIDA and ASPECT Missions

In this chapter a detailed description of the Asteroid Impact & Deflection Assessment (AIDA) mission is given. The mission serves as a base of this master thesis. The AIDA mission is a joint collaboration between ESA, NASA, the German Aerospace Center (DLR), Observatoire de la Côte d’Azur (OCA), and the John Hopkins University Applied Physics Laboratory (JHU/APL). This mission, as stated in the introduction, consists of separate spacecraft which will travel to the near-Earth binary asteroid Didymos in order to test a kinetic impactor technique to deflect an asteroid. [25]

The binary system consists of a primary body of approximately 800 meters across and a secondary body of 150 meters. The kinetic impactor intends to hit the secondary. Its size is more common among the asteroids that represent a hazard to Earth. Therefore, this test would provide more relevant information. [29] The mission carries out science-motivated tests and it represents the first of its kind. It would investigate the surface, the subsurface and the internal properties of a small asteroid system. Allowing at the same time, the demonstration and testing of new technologies that can be useful in other space projects. [25, 30] Two main spacecraft are being developed for this purpose:

- An asteroid impactor by NASA under the name Double Asteroid Redirection Test (DART).
- An asteroid rendezvous spacecraft by ESA under the name Asteroid Impact Mission (AIM).

The AIM spacecraft is set to rendezvous with the Didymos asteroid to characterise the smaller of the two binary components, defined as Didymoon, before and after the impact of the DART spacecraft. AIM will measure the physical and dynamical properties of the system and it would determine any change produced by the impact. On the other hand, aided by a camera and a complex navigation system, the DART spacecraft will crash itself into the secondary at approximately 6 km/s. The collision is expected to change the orbit speed of Didymoon around the primary body by 1 percent. [30, 29]

Both missions’ schedules are synchronised in contemplation of the joint campaign, although they are able to perform independently. AIM is planned to be launched in October/November 2020, reaching the Didymos system in April 2022. DART would be launched in December 2020 and it would impact by the end of September 2022. The AIM spacecraft will arrive at Didymos before DART’s impact and with its array of instruments it would provide the first analysis and high-resolution imagery of the binary asteroid. The goal is to measure the masses, the densities and the shapes of the bodies while it is orbiting and observing at a safe distance. After the impact, the AIM spacecraft will try to determine the momentum transferred by observing the size of the crater and redistribution of the material (structure and composition). AIM will also deploy a lander, defined as Mobile Asteroid Surface Scout or MASCOT-2, which will characterize Didymoon before, during and after the impact of the DART spacecraft [29]. Figure 5 portrays the mission concept. Here, two more objects with

labels: "CubeSat 1" and "CubeSat 2" represent the side spacecraft mission defined as the Cubesat Opportunity Payloads (COPINS). [25, 30, 29]

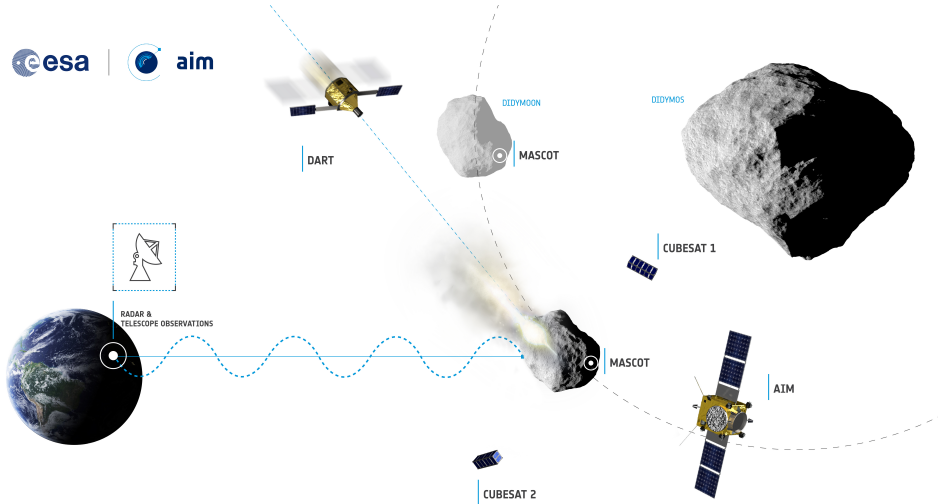


Figure 5: AIDA mission concept infographic [25].

In addition to the two main spacecraft, AIM is capable of accommodating two three-unit-CubeSats to complement its mission. The small size of a CubeSat allows an affordable opportunity for research institutes, small companies and/or universities to cooperate in this deep space mission [25]. The Asteroid Spectral Imaging Mission (ASEPCT), a three-unit CubeSat, has been proposed as the complementary or support mission of the AIM. The details and requirements are given in the next section.

To summarise the AIDA mission, the main goals include the asteroid system characterisation; the demonstration of the deflection method; and the definition of: the orbital state, the rotation state, size, shape, gravity, geology and internal structure of the asteroid system. The categorisation of these outcomes are depicted in Figure 6. The information obtained would have important implications that will enhance the comprehension of the mechanical response of an asteroid and the impact cratering process at a real scale. Consequently, a better understanding of the collisional evolution of these bodies and the Solar System in general. At the same time, the measurements of a close encounter can be compared to ground-based data. Thus, allowing an improvement of data interpretation and of calibration methods for instruments on Earth. The results will also provide an insight into the force required to deflect the orbit of any incoming asteroid, permitting the planning of future defence strategies. [25, 30]

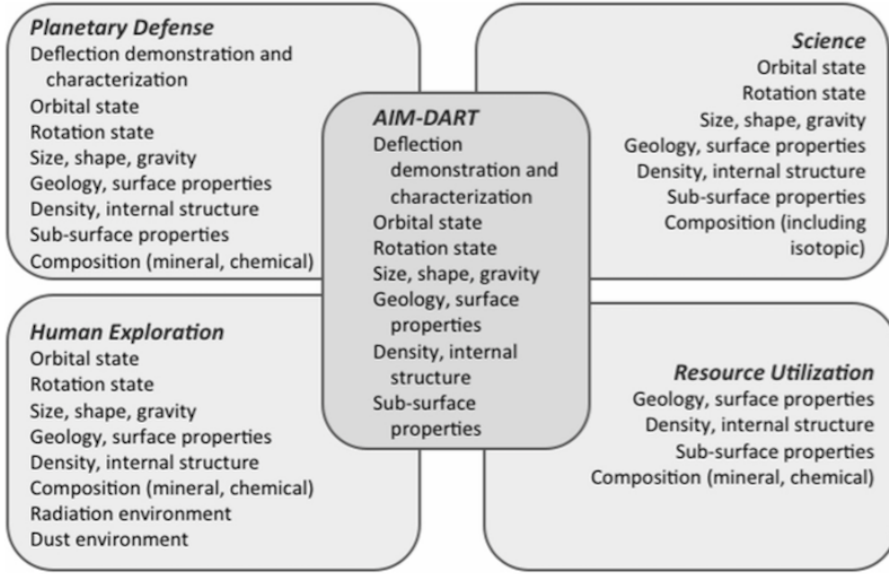


Figure 6: AIDA mission objectives. It would provide knowledge concerning several disciplines [30].

3.1 Details and Requirements of the ASPECT Mission.

The use of small CubeSats is growing continuously since their first launch in 2000 by the Stanford University as part of a demonstration of feasibility and practicability of new space projects [31]. This generation of satellites is now being developed by universities and organizations who are looking for space experiment platforms that have a low construction and launch costs. The AIM is planned to accommodate two CubeSats, providing the first opportunity to operate these devices in a deep space mission. These CubeSats would host a group of sensors that would complement and expand the scientific return of the mission. They would add a close-up look at the composition of the surface of the asteroid, the gravity field and an assessment of the impact created by DART. Furthermore, the AIM would also test an inter-satellite communication network in deep space which will also be used as part of the navigation system of the small payloads in the vicinity of Didymos. [31, 25]

VTT Research Centre of Finland along with Aalto University and the University of Helsinki, have proposed the Asteroid Spectral Imaging Mission (ASPECT). The ASPECT is a CubeSat with a visible/near-infrared spectrometer. It has the purpose of assessing the composition of the asteroid and observing the effects of space weathering and metamorphic shock after the impact. If successful, the technology used here would establish the base of several applications in environments of hard radiation beyond the common low-Earth orbits at an affordable cost. [5, 25]

The ASPECT satellite is a three-unit CubeSat (3U) and each unit is designed to allocate a subsystem: 1U is the payload itself, a spectral imager, 1U corresponds to

the avionics module, and the last 1U is reserved for the propulsion system [5]. An overview with the schematic and basic characteristics of the satellite can be seen in Figure 7. Here, the most important information in respect of the thesis is the mass of the spacecraft, the level of accuracy of its attitude control system and of course its measurements. Furthermore, a determination of the exact center of mass is essential for the upcoming calculations and models. Nonetheless, this datum will not be available until a final flight model is constructed. In the meantime, its geometrical center is considered as its center of mass.

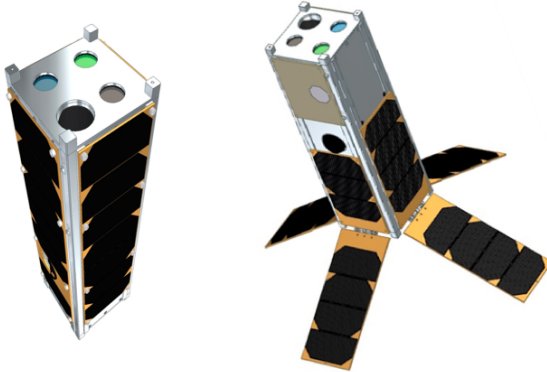


Figure 7: ASPECT platform concepts with two different arrangement of the solar panels [5].

ASPECT Satellite	
Mass [kg]	4.5
Power [W]	8-15
Attitude determination [°]	<0.1
Attitude control [°]	<1
Dimensions [cm³]	34x10x10

Table 1: Basic platform characteristics required in the ADCS design. [5]

The objectives of the satellite mission can be divided into scientific objectives and technical objectives. Knowing the goals will help to clarify the operation modes, as well as the position and orientation of the satellite. The scientific objectives are [5]:

- Mapping the surface composition of the Didymos system.
- Photometric observations and modelling of the Didymos system under varying phase angle and distance.
- Evaluation of the space weathering effects on Didymoon.

- Identification of local shock effects on Didymoon based on spectral properties of the crater after the impact.
- Observation of the plume produced by the impact of the DART spacecraft.
- Mapping the global mass transfer between the primary and the secondary body.

The technical objectives are [5]:

- Demonstration of a CubeSat autonomous operation in a deep space environment.
- Navigation in the vicinity of a binary asteroid.
- Demonstration of a joint spacecraft operation.
- Demonstration of spectral imaging of asteroid materials.

The expected science results would complement those of the AIM spacecraft. The composition and homogeneity of the Didymos asteroid will be measured. This would improve the understanding of the origin and evolution of a binary system. The data obtained would also permit to know more about the processes that the surfaces undergo while being in a zero-atmosphere and interplanetary environment. [5]

The idea is to establish the type of orbit that would need to be achieved to carry on the mission. The payload of the satellite includes a set of spectral imagers for different wavelengths. Namely, a Visible, a Near-Infrared and a shortwave-infrared imagers (VIS, NIR and SWIR respectively). The scientific and technical requirements are: a spectral range of $0.7\text{-}2.3 \mu\text{m}$; a spectral resolution of 45 nm; a spatial resolution of the VIS of 1 m/pixel or better; and eight equally spaced (max 45°) observations of Didymoon. Under this circumstances the ASPECT team determined that an optimal orbit to do the measurements would be a circular orbit with a semimajor axis of approximately 4.1 km around the primary. A slight inclination of the orbit is also considered. [5]

The Figures 8 and 9 illustrate the required orbit of the ASPECT satellite. Determining an orbit is fundamental for the design of ADCS. According to Newton's law of gravity: the distance between each body defines the gravity force that they exert to or feel from another body. As a result of this interaction, the motion and disturbance models such as: the gravity field, the gravity gradient and third-body perturbations can be implemented. [1]

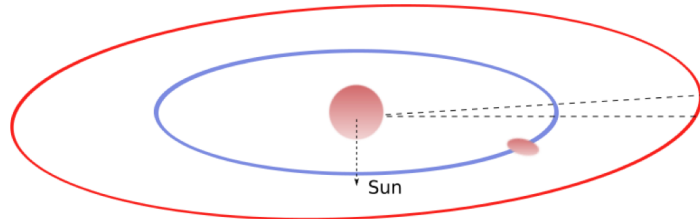


Figure 8: Representation of the operation orbit of the spacecraft. Radius of 4.1 km and a slight inclination. [5]

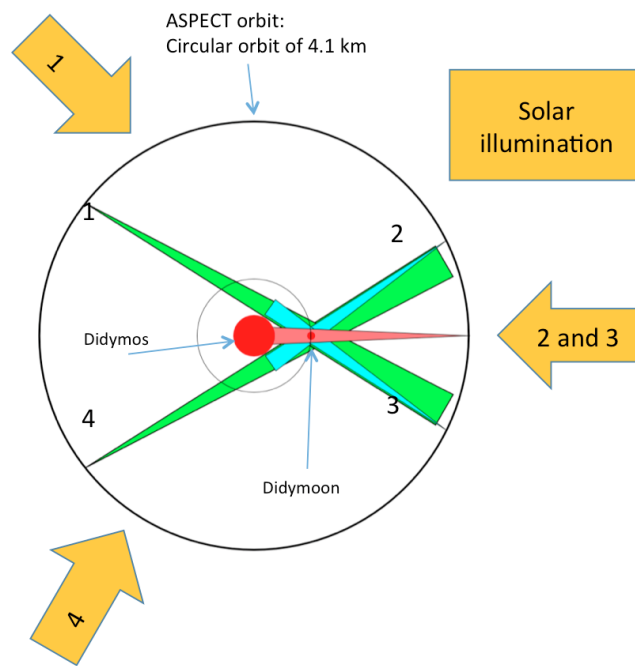


Figure 9: Top view of the orbit plane, this represents the geometry needed for the imaging [5].

Besides the orbit of the local system, it is indispensable to know the orbit respect to the Sun. The AIM spacecraft will bring the ASP CET satellite in the proximity of Didymos. However, once deployed, the CubeSat would be on its own while navigating. Hence, knowing the ephemeris of the asteroid system (in other words, the distance to the Sun at specific times) is imperative to make the pertinent calculations related to gravitational and non-gravitational disturbances. The solar radiation, a non-gravitational effect, would apply a pressure on the surfaces of the satellite directly proportional to the distance. Additionally, gravity forces exerted by other massive bodies, like the Earth or Jupiter, might need to be considered; therefore, their relative distances should be known too. [1, 25]

The distances of the bodies of interest depend on the dates of the mission. The optimal time occurs in October 2022, when the asteroid passes close from the Earth [25]. The Figure 11 shows how the distance of the spacecraft would vary throughout the mission, the dotted lines represent the arrival to the system, the expected end and the foreseen extension.

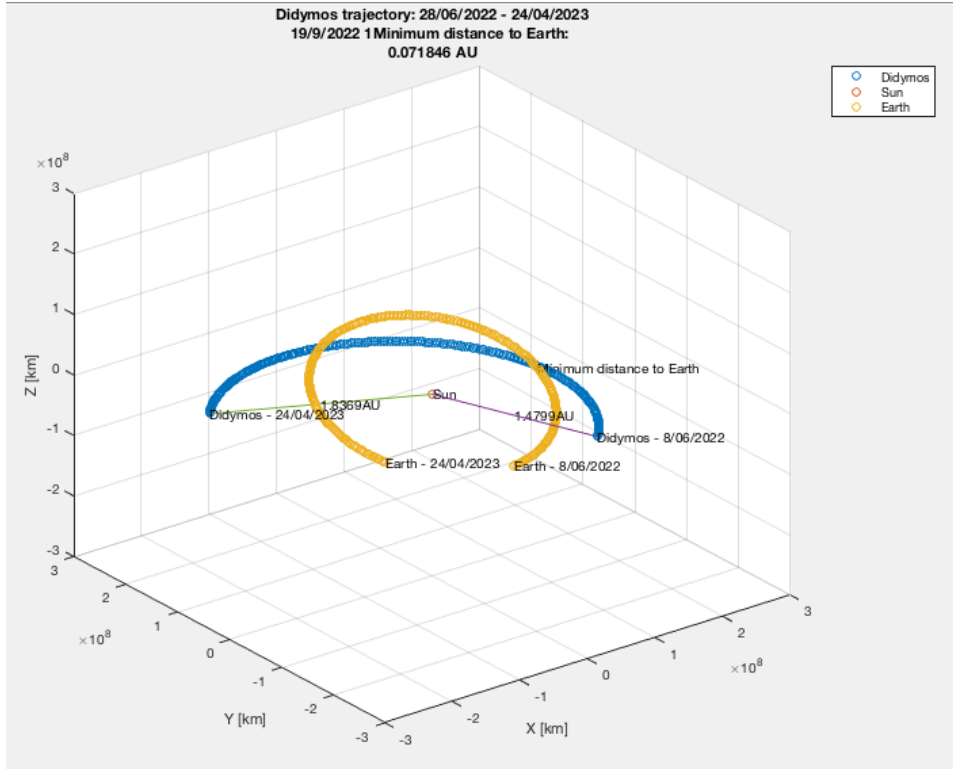


Figure 10: Didymos ephemeris 28/06/2022 - 24/04/2023. Critical distances during the mission are 1 AU and 1.5 AU.

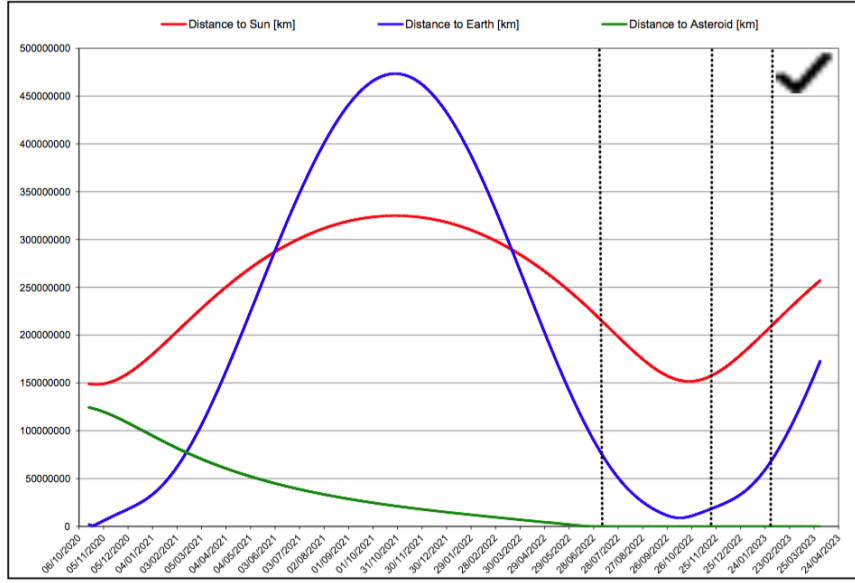


Figure 11: Distances from spacecraft. Dotted lines represent arrival to asteroid system, nominal end of mission and foreseen extended end of mission. On x-axis is time and y-axis represents the distance to Earth in km [32].

4 Theory of Small Bodies: Asteroid Systems

In order to study the dynamics of a spacecraft in the proximity of an asteroid, it is paramount to understand the sub-set of properties of these bodies which define the environment around them. For instance, the mass, the density, size and morphology are needed for the modelling. In this chapter, these properties are portrayed, as well as their connection with the orbits, the rotation states, gravitational field and the perturbations that act on a spacecraft in their vicinity. Afterwards, we will revise the same properties of the Didymos system according to the latest observations and studies. Basically, all the information needed for the modelling and the simulation of the Didymos asteroid environment are presented.

4.1 Modelling Small Body Environments

There have been numerous papers and proposals trying to describe exploration activities revolving small bodies, but not many have addressed a clear focus on the requirements of a spacecraft when they arrive to these small bodies. However, by understanding the fundamental mechanics of a small body, this becomes a feasible goal. [1]

4.1.1 Mass and Density

An essential property of a small celestial body is the value of its mass, as it controls the gravitational attraction that it exerts on a spacecraft. Besides this, density is a more crucial parameter. According to text [1], these parameters can be calculated as follows:

$$\delta = M/V, \quad (1)$$

where δ is the mean density, M is the body mass and V is the total volume. However, an exact shape, thus the volume, is not always entirely known and this is why the concept of mean radius R , appears. It is defined as the radius of a sphere of equal volume or the geometric mean of the body's size:

$$R = (3V/4\pi)^{1/3}. \quad (2)$$

This measure can roughly tell how close a spacecraft can approach and it also helps us to see why the period of an orbit is defined by its density and body radii, rather than by its total size. [1] The 3rd Law of Kepler states that the period of an orbit is:

$$T = \frac{2\pi a^{3/2}}{\sqrt{GM}}, \quad (3)$$

where T is the period, a is the semimajor axis of the orbit, M is the total mass of the system and G is the gravitational constant whose value is $6.673 \times 10^{-8} \text{ cm}^3 \text{ g}^{-1} \text{ s}^{-2}$. But, equations 1 and 2 can be replaced in the last one, obtaining the next expression [1]:

$$T = \sqrt{\frac{3\pi}{G\delta}} \left(\frac{a}{R}\right)^{3/2}. \quad (4)$$

This proves that the orbit period around a body depends on its density and not in the size when it is written in terms of body radii. In other words, bodies with similar densities will mirror similar orbit periods. In a binary system, it is possible to infer its density by observing its orbit period. This density would be the bulk density and for asteroids, it is commonly found in the range of 1 g/cm³ - 5 g/cm³. [1] Although, in a binary system the two bodies may have very different densities and one of the key questions in the AIDA mission would be to precisely determine the reason behind this.

4.1.2 Spin State

Another property that controls how a small celestial body interacts with an orbiting particle, is the spin dynamics. Spin dynamics refers to the rotation state or more precisely: the angular momentum. Small bodies are divided into three classes: uniformly rotators, complex rotators and synchronised rotators. Relevant for the study is the orientation of the body's total angular momentum because it is assumed to be conserved. Binary asteroids, being composed by two bodies, exhibit usually a uniform rotation of the main body, while the secondary displays a synchronous rotation. Moreover, the angular momentum vector is believed to be parallel to the one of the Sun in a heliocentric reference frame. [1, 30]

Being a uniform rotator means that the body would revolve around its maximum moment of inertia as it is the minimum energy rotation state [1]. Thousands of observations have revealed that asteroids upper limit of spin period is around 2.4 hours, which implies also a range for the density and their body structure (either made of rubble piles or only by a monolithic rock). Spin rate tends to change over time; in particular, because of certain radio-thermal perturbations such as the Yarkovsky-O'Keefe-Radzievskii-Paddack effect (YORP). This effect is a mechanism that may speed up or down the spin state of a small body with an irregular shape due to the absorption of sunlight and then emission of the same in the form of thermal radiation. Nonetheless, the time-scale of the dynamics provoked by this effect is so large compared to other effects that it is not considered for the design of spacecraft missions. [1, 33]

The other type of rotator is the synchronous rotator. Here, the body's orbital period respect to a main body is equal to its own rotation around the axis of its largest moment of inertia. For instance, this happens in the Earth and Moon system or in the great majority of the binary asteroid systems [1]. There is a third type of rotator, a complex rotator, where the body is specified as "tumbling"; however, when such situation happens, there are other effects like the tidal effects that would spin-up or de-spin the body in order to make them go into a 1:1 spin-orbit, thus synchronous system. [1, 34]

4.1.3 Shape and Morphology

Planets and planetary natural satellites generally resemble a spheroid; conversely, asteroids detailed structure is more complex. Asteroids are normally defined as ellipsoids. [35, 36, 1] Three fundamental specific shape models exist. First, a simple tabulation method of radius, longitude and latitude; second, the general polyhedra with triangular facets; and finally, the quadrilateral-implied format. Although, for gravitational and orbit analysis, lower resolution models with the overall morphology of a body's shape would suffice, therefore no more explanation of the first ones will be given here. Instead, a brief outline of the shapes based on radar and imagery observations are described. [1]

The most accurate models are images based on the combination of visual imagery taken from different phase angles. The best models are constructed out from data obtained by a rendezvous spacecraft, but flyby missions can occasionally provide good full and partial shapes of asteroids. Further, there are shapes also based on radar range-Doppler imaging: these images are taken by the Arecibo or Goldstone radio antenna when the small bodies pass close enough to our planet. [1, 30] This process allows resolutions of tens of meters and also provides an estimation of the spin state, therefore density and size as well. The last simple form of shape construction is through a light curve analysis. It is a photometric observation of the body that measures the variation in the reflected light; then, by assuming an albedo, the body can be tracked as a function of time. [1] The Figures 3 and 14 show examples of these shape modelling techniques. These models do not contain a great detail. Although they are sufficient to estimate the gravitational field of an asteroid up to second degree which is what has been done so far about the Didymos system and what is needed for the purpose of this thesis.

4.1.4 Gravitational Potential: Spherical Harmonics Model

One of the main characteristics of an asteroid, or of small celestial bodies in general, is the non-regular shape of the body. This non-homogeneous distribution of mass has a strong impact in the motion and attitude of an orbiter around it [37]. Previous missions to the asteroid Eros, Castalia and Toutatis have helped in the understanding of the gravitational field. The gravity field of an asteroid can be represented by a second-degree and second-order equation [37, 35, 36, 1].

The potential, U , is given by the integral of a differential mass element over the entire body that composes the primary body of the asteroid [37, 1]:

$$U(\mathbf{r}) = G \int_{\beta} \frac{dm(\boldsymbol{\rho})}{|\mathbf{r} - \boldsymbol{\rho}|}. \quad (5)$$

Here, \mathbf{r} represents the distance to the center of mass of the asteroid. Then, as shown in Figure 12, $\boldsymbol{\rho}$ is a position vector of the differential mass element dm , β corresponds to the set containing all the mass elements that constitute the body. The gravitational potential satisfies Laplace's equation: $\nabla^2 U = 0$ for the case inside the body and $\nabla^2 U = -4\pi G\sigma$ for the case outside the body, where σ means the local density [1].

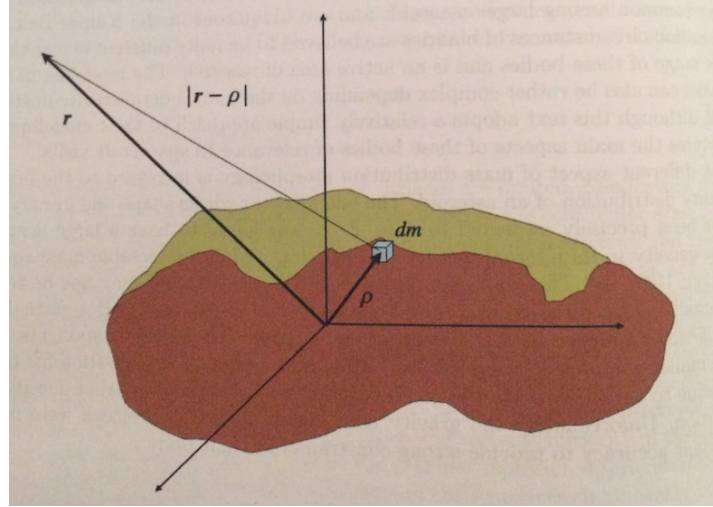


Figure 12: Mass distribution geometry [1].

The gravitational potential of a non-spherical body can be approached in many ways and mathematically, any solution that satisfies the Laplace equation is valid. A good approximation to describe the gravitational field of a small body is the spherical harmonics model, also known as asteroid zonal harmonics when applied to this particular bodies. [37, 1, 38]

Laplace's equation can also be solved by changing the $\mathbf{r} = x\hat{\mathbf{x}} + y\hat{\mathbf{y}} + z\hat{\mathbf{z}}$ vector into spherical coordinates:

$$r = \sqrt{x^2 + y^2 + z^2}, \quad (6)$$

$$\sin \theta = \frac{z}{r}, \quad (7)$$

$$\tan \lambda = \frac{y}{x}, \quad (8)$$

where θ is the latitude and λ is the longitude. Next, by using the separation of variables method to obtain the general form of the spherical harmonic potential:

$$U(r, \theta, \lambda) = \frac{GM}{r} \sum_{n=0}^{\infty} \sum_{m=0}^n \frac{R^n}{r^n} P_{nm}(\sin \theta) (C_{nm} \cos(m\lambda) + S_{nm} \sin(m\lambda)), \quad (9)$$

where R is the mean radius of the body, C_{nm} and S_{nm} are spherical harmonic coefficients and P_{nm} is the Legendre polynomial of degree n and order m . This spherical harmonic coefficients can be found in the next way [37, 1]:

$$C_{20} = \frac{1}{5R^2} \left(c^2 - \frac{a^2 + b^2}{2} \right), \quad (10)$$

$$C_{22} = \frac{1}{20R^2} (a^2 - b^2). \quad (11)$$

These formulas are valid in the case of a triaxial ellipsoid with a homogeneous mass distribution and semi-axes a , b and c as depicted in Figure 13.

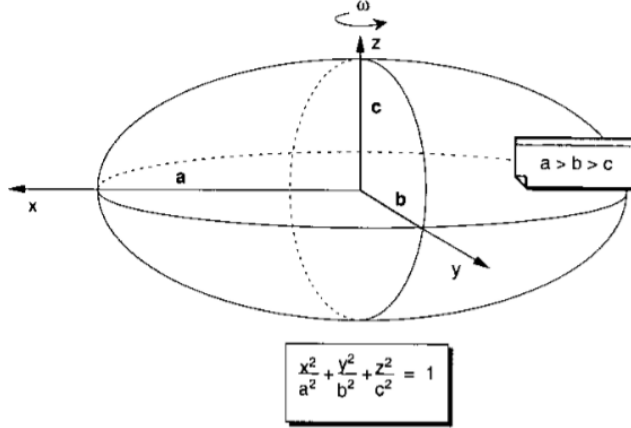


Figure 13: The triaxial ellipsoid [35].

In order to get the full gravitational potential, the Legendre polynomials, P_{nm} , can be used. In this case, second order polynomials are used. First, the general form is:

$$P_{nm} = (1 - u^2)^{\frac{m}{2}} \frac{d^m P_n(u)}{du^m}. \quad (12)$$

Second, from Appendix B the case for the second order polynomials states:

$$P_{20} = \frac{1}{2} (3uP_{10}(u) - P_{00}(u)) = \frac{1}{2} (3u^2 - 1), \quad (13)$$

$$P_{22} = 3(1 - u^2)^{\frac{1}{2}} P_{11} = 3(1 - u^2); \quad (14)$$

where $P_{00}(u) = 1$ [39]. Finally, the S coefficients are found to be $S_{21} = 0$ and $S_{22} = 0$. This happens when the Z-axis is aligned with the shortest axis of the ellipsoid; thus, with the maximum moment of inertia [40]. Integrating all of the above gives us the gravitational potential, $U(r, \theta, \lambda)$, as follows:

$$U(r, \theta, \lambda) = \frac{GM}{r} \left[\frac{1}{2} (3\cos^2\theta - 1) C_{20} + 3(1 - \cos^2\theta) C_{22}\cos(2\lambda) \right], \quad (15)$$

which can be used to calculate the attraction force that would affect the motion of a particle or spacecraft. The spherical harmonics model has some limitations though, as it cannot be used when one wants to consider the gravitational potential at a very close distance of a body with non-regular shape.

However, there are many more accurate models to describe the gravitational potential. Three suitable examples are the ellipsoidal harmonic expansion and two more closed-forms of the gravitational potentials: the constant density ellipsoid and the constant density polyhedron. The first one, is a very similar approach to the spherical one, but it mitigates the divergence effect in the boundaries; although, it is more complex. The closed-form models do not suffer from the same limitations, but they heavily rely on knowing the specific shape of the body and on strong assumptions about the density distribution. [1] This detailed information of the Didymos system is not available yet, but it should be kept in the records to build a more accurate gravitational potential model in the future.

4.2 Dynamical and Physical Properties of Didymos

After recounting all the main properties that are necessary to model the space environment; next, they can be associated to the Didymos system.

The near asteroid Didymos is an Apollo asteroid, which means that its orbit around the Sun has a larger semi-major axis than the Earth (1 AU), but whose perihelion distance is less than the aphelion of the Earth (< 1.017 AU). Didymos was first acknowledged on April 11th 1996, although it was not until 2003 that, thanks to new observations, it was discovered as a binary system. The main physical and dynamical properties were derived by photometric and radar observations. [41, 30] Tables 2 and 3 summarise this information. It is important to know them in order to understand the dynamics of a spacecraft orbiting the system and the perturbations associated.

Didymos	Primary	Secondary
Mass [kg]	5.24×10^{11}	3.45×10^9
Radius [km]	0.385	0.163 ± 0.018
Bulk density [km m^{-3}]	2, 100	–
$C_{2,0}$ un-normalized	-0.023	–
$C_{2,2}$ un-normalized	-0.0013	–
Spin period [h]	2.259	–

Table 2: Didymos system basic properties [41, 42].

Orbital Elements at Epoch (2016-Jul-31.0)	
Eccentricity	0.383971
Semi-major axis [AU]	1.64435
Perihelion distance [AU]	1.013129
Inclination [°]	3.4077
Longitude of the ascending node [°]	73.22647
Argument of perihelion [°]	319.2241
Mean anomaly [°]	17.34152
Time of perihelion passage [JED]	2457563.4 (2016-Jun-23.9)
Period [days]	770.173
Mean motion [°/day]	0.46742742
Aphelion distance [AU]	2.27556
Mutual orbit	
Orbital period [h]	11.9
Semi-major axis [km]	1.178
Eccentricity	0.02
Orbital pole (λ, β) [°]	(300, -60)

Table 3: Didymos orbital elements and mutual orbit properties [43, 42, 41].

A critical parameter for determining the properties of the system is knowing the state of their mutual orbit. The primary gyrates at a uniform rotation period of 2.26 h \pm 0.00001 h [30] and the secondary body is presumably orbiting synchronously in a retrograde form on the equatorial plane of the primary body with a variation of its inclination of less than 0.003°. The determined orbit period for this case corresponds to 11.920 h+0.004 h/ – 0.006 h. Correspondingly, the secondary-to-primary mean diameter ratio is estimated to be 0.21 ± 0.01 , thus constraining the orbit with a low eccentricity of ~ 0.02 ; almost circular [30, 41]. In addition, it is also assumed to be a triaxial ellipsoid with its axial ratios a/b and b/c being between 1.1 and 1.5. [30]

Moreover, by using the radar and photometric observations, data taken at Arecibo and Goldstone, an image of the current model or shape was derived from the same measurements. With this analysis, the diameter of both bodies was estimated to be 0.78 km and 0.163 km with an uncertainty of ± 10 percent and a total mass of 5.3×10^{11} kg. Likewise, the distance between both centers of mass, semimajor of their mutual orbit, was estimated to be ~ 1.18 km. [30] Figure 14 depicts a representation of the asteroid system with the aforementioned characteristics.

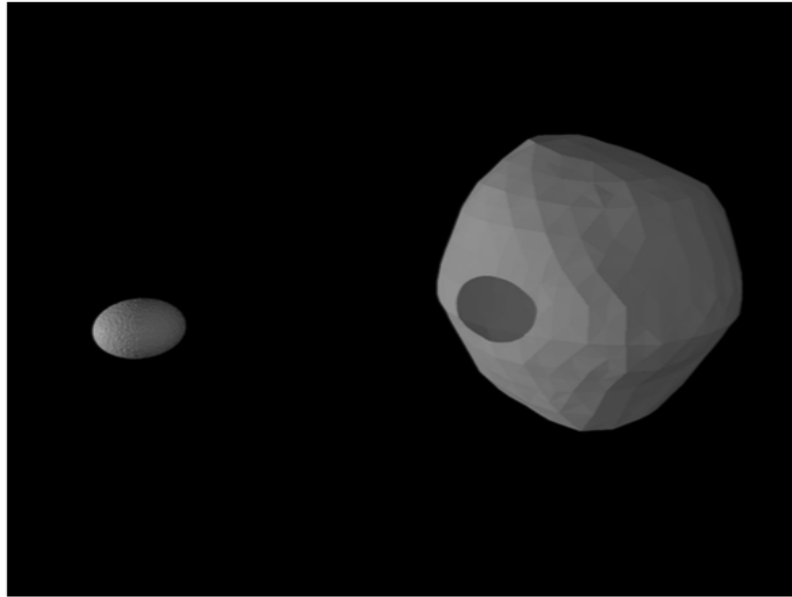


Figure 14: Preliminary shape model of the Didymos system, obtained by combining models reconstructed from radar and photometry data, with a diameter of 780 m. Didymoon is assumed as an ellipsoid with a major axis of 170 m [41].

Other physical properties than the mean diameter and mass have not been constrained by the observations. Extra assumptions need to be taken carefully in consideration. However, even under some uncertainties, reasonable models and other parameters or state estimations can be done. It is assumed that Didymoon is in synchronous orbit around the primary, but the rotation state is not constrained by observations and it may be unstable. Also, it is speculated that the asteroid is composed by regolith material and that it is very close to its critical rotation state. The impact of the DART spacecraft will definitely affect dynamics of the system that may change the environment in which the ASPECT satellite would operate. [30]

A crater would be produced on the secondary. The size and morphology depend on the under layers or sub-surface structure and mechanical properties. Nevertheless, a large-scale restructure of the celestial body is improbable to happen, since the energy level of the impact is several orders of magnitude below a catastrophic disruption. On the other hand, the dynamical properties will be affected. In particular, the mutual orbit period will be modified, but this change would not go beyond more than a few minutes according to preliminary studies. [30] Another concern is the fate of the ejecta produced by the impact, because it may have implications on the safety and operations of the spacecraft. This redistribution depends strongly on the properties of the surface layer. Although the solar radiation pressure, the solar tides and the gravitational environment will keep the forces balanced. Hence, no large redistribution would happen. The debris cloud around the asteroid can last from days to months. [41, 30]

The analysis of the Didymos system also include its thermal properties. These govern part of the non-gravitational perturbations, like the Yarkovsky effect. Nonetheless, this effect along with others, such as the effect of solar and Earth tides or the orbiting debris may be neglected. They are considered long-term perturbations. These perturbations would not affect, in a considerable scale, the attitude and orbit of a spacecraft stopping over a couple of months. The analysis of these long-term dynamics are of interest, but they are not relevant over short lifespan corresponding to the mission design of a spacecraft. [1] However, more information about these effects may be found in [41, 30, 44, 33].

In summary, this chapter defined the characteristics to consider of a small body in order to do the modelling the environment: mass, density, spin state, gravitational field, size, among other parameters. These properties were determined for the Didymos system with radar and photometric observations. Nevertheless, there have been many assumptions used during the analysis. These may change in the upcoming years before the AIM mission is launched, if more accurate measurements are done. Similarly, as the AIM spacecraft approaches to its target, probably better estimations of the same properties could be made. Then, the GNC of all spacecraft should be adjusted accordingly.

5 Modelling of a Spacecraft Orbiting a Binary Asteroid System

Modelling complies the task of identifying the mathematical relationships that describe a real-world system. With the support of software and hardware, this virtual representation of a system can be tested under a wide range of conditions to analyse its behaviour over time. In other words, it is called a simulation. Modelling and simulation can improve the quality of the design by helping us to identify and reduce the errors found in the early design phases. They allow us to test conditions that may be difficult to reproduce only with prototypes; which is the case of space systems. [45, 9]

In order to design the ADCS, an environment where the spacecraft will be orbiting should be characterised. This environment consists of several models that will be detailed in this chapter. The first step is to define the reference frames, where the vectors can be represented in space. In addition, different coordinate systems are chosen to ease the calculations. The next step requires the modelling of the space environment associated to our system. This includes an ephemeris model, which is the position of the astronomical bodies of interest at a given time; and the modelling of the disturbances affecting the satellite in the vicinity of the binary asteroid. Furthermore, the dynamics and kinematics of the spacecraft are modelled to determine how it is affected by the environment. [4]

5.1 Coordinate Systems

When working with the ADCS of a spacecraft, its orientation and orbit need to be determined. A coordinate system shall become the basis for its attitude representation, and because a satellite can be observed from multiple perspectives, suitable reference frames for attitude determination and control purposes need to be defined. In this project the reference frames are defined as right-handed 3-dimensional Cartesian coordinate systems, which are described by three mutually orthogonal unit vectors. Subsequently, it is possible to model the satellite and the environment surrounding it. A brief overview of these reference frames is presented, although for a deeper explanation, more information is available in the literature [46, 47, 4]. The list below shows the reference frames used in the simulation.

- Asteroid Inertial Reference Frame - (I)
- Asteroid Centered Fixed Reference Frame - (AF)
- Orbit reference Frame - (O)
- Spacecraft Reference Frame - (S)
- Heliocentric Reference Frame - (H)
- Controller Reference Frame - (C)

Asteroid Inertial Reference Frame. First, an inertial reference frame is required to have a non-accelerating point of view, in order for Newton's laws of motion to be valid. This frame can be extended to any other frame. A precise inertial frame would be a Sun centered frame. However, it would not be ideal because the Sun orbits the Milky-way and so forth until reaching the center of the universe (not possible to determine). Since no perfect inertial reference frame exists, choosing the Didymos system is the best way to proceed in this project. This would ease the calculations too. This reference frame is called (I). The asteroid inertial reference frame depicted in Figure 15 would be accurate enough for the attitude analysis. [4, 46, 48]

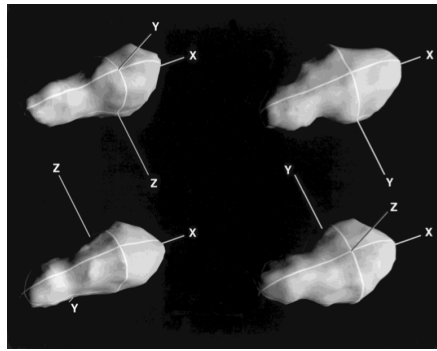


Figure 15: Asteroid inertial reference frame. Coordinate axes shown in four perspectives [49].

Asteroid Centered Fixed Reference Frame. Some calculations are simplified by utilising a reference frame that rotates at the spin period of the primary body. The orbit propagator and some environment disturbances depend on this specific relative position between the spacecraft and the asteroid. For this reason, this frame, called (AF), is introduced. The z-axis of this frame is aligned with the maximum moment of inertia of the asteroid. Being a uniform rotator, this axis is set as perpendicular to its orbit plane. The x-axis is orthogonal to the z-axis and it is pointing to a fixed point on the surface of the asteroid. Currently, an arbitrary point can be chosen as long as rests on the orbit plane of the asteroid. Finally, the y-axis results from the cross product of these two. [41, 1, 4]

Spacecraft Reference Frame. The spacecraft reference frame (S) is defined by its origo fixed at a point relative to the body of the satellite. It can also be called spacecraft-fixed or spacecraft body frame. It is used to determine the orientation or alignment of the various spacecraft instruments. [4, 48] The payload of ASPECT requires to point at a certain direction. Also, its center of mass will probably not be located in its geometrical center. Therefore, it would be convenient to define a second reference frame, the controller reference frame (C). In combination, these two would be used for the attitude determination and control system. Figure 16 shows the reference frame (S). As an example, it has its center in one of the corners of

the satellite, but it could be established at any part. The axes form a right-handed coordinate system.

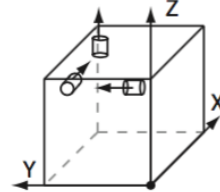


Figure 16: Spacecraft reference frame [4].

Orbit Reference Frame. The orbit reference frame, (O) is a non-inertial reference frame with its origo in the center of mass of the spacecraft. This is system is also referred as the roll-pitch-yaw system [46, 47]. The frame axes are aligned with the nadir vector. This vector is pointing from the satellite to the orbiting the asteroid. The second vector points along the orbital velocity vector of the spacecraft. The third vector is formed with the cross product between the first two. This system is shown in Figure 17.

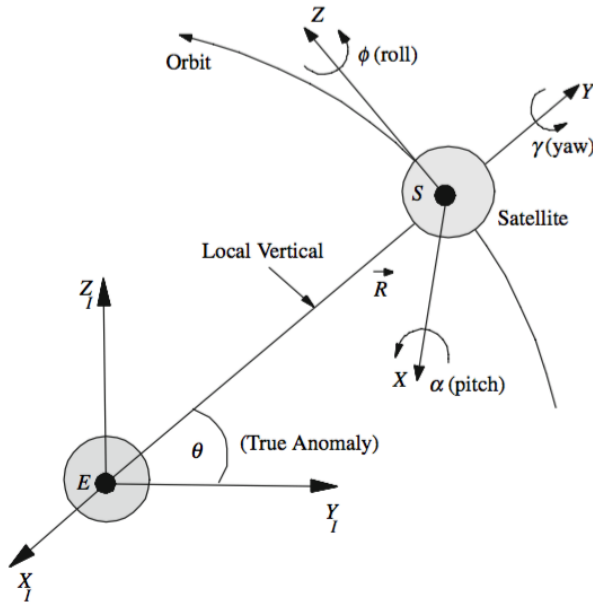


Figure 17: Representation of the orbit reference frame with axes: X, Y, Z with origin in S , the orbiting satellite; and the inertial reference frame with axes: X_I, Y_I, Z_I with origin in E , the asteroid [37].

Controller Reference Frame. As mentioned above, a controller reference frame, (C), is convenient to calculate the dynamics. All the products of inertia disappear and only the main diagonal of the inertia matrix remains with non-zero values. This system is shown in Figure 18, the origo corresponds to the center of mass of the spacecraft. The axes are defined respect to the major and minor moments of inertia of the satellite, the x -axis and the y -axis. The z -axis results from the cross product of these two forming again a right-handed Cartesian system. This system is necessary, because the satellite does not have a spherical shape nor a uniform mass distribution. [4]

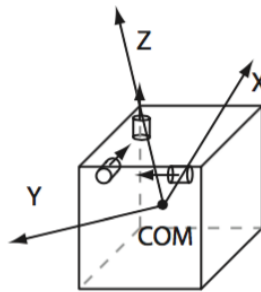


Figure 18: Controller reference frame [4].

5.1.1 Coordinate System Transformations

There are different mathematical representations to describe the relative orientation of each reference frame respect to the other. Literature says that common representations include the direction cosine matrix, the Euler angles, the Euler axis/angle and the unit quaternions representations. The Rodrigues parameters is another system which is less used. Each representation has its own advantages and shortcomings. The most general attitude representation is the rotation matrix. It is a simple orthogonal matrix which is operated with just matrix algebra, but requires more computation. It is composed by 9 elements which make it redundant and it might also lead to singularities. Euler angle and Euler axis/angle are easy to interpret, because there is a direct physical representation. This characteristic makes it intuitive for users when working with the input-output variables of attitude systems. However, they are also prone to singularities and non-unique solutions. [48, 46, 47]

The last mathematical representation revised and used for most of the calculations during the simulation are the unit quaternions. Quaternions are 4-element-based representations of attitude transformation and they work under their own mathematical operators. They share some properties with matrix algebra, but they have reduced redundancy, 4 elements instead of 9. This is more suitable for computer calculations and they provide a singularity-free representation of the kinematics. Nonetheless, their physical interpretation seems meaningless, since it is not intuitive. For a better

insight of quaternions, appendix A describes the fundamental algebra of quaternions. [48, 46, 47]

5.2 Ephemerides

In astronomy and celestial navigation, the collection of position and velocity data of a natural or an artificial object at a given period of time is called an ephemeris. Ephemerides are fundamental for the navigation of spacecraft and any type of astronomical observation. Modern ephemerides are obtained using computers that solve mathematical models of motion which also consider the continuous update of data provided by new observations. For the last couple of decades, NASA's JPL has performed this task for planets, planetary satellites, comets and asteroids [50].

This information is required as input for the disturbance model, since the magnitude of the perturbations are directly related to their relative position respect to the satellite [1]. For this reason, the ephemerides corresponding to certain bodies are fundamental. In this mission, the bodies of interest are the Sun, the Earth and Jupiter. They exert the strongest influence on both, the asteroid system and the satellite [42].

5.3 Disturbances Acting on the Spacecraft

This section reviews the torque and force disturbances that normally act on a spacecraft. Ultimately, the performance of the spacecraft will depend on the magnitude and direction of these torque disturbances, because they change the angular momentum of the satellite. The disturbances can be either internal or external. Actuators in a spacecraft are used to counter the external disturbances, therefore it is important to know how considerable their impact would be in order to propose a suitable actuator system. [7]

Table 4 shows the common acknowledged disturbances when designing a spacecraft.

Disturbance	Source	Description
Solar Radiation Pressure	The Sun	The disturbance torque and force which depends on the exchange of momentum between the photons coming from the sun when they burst into the surface of the spacecraft.
Gravity Gradient	Inertia	When a satellite has off-diagonal inertia terms due to its distributed nature, it will produce a body fixed torque.
Gravitational potential	Irregular shape of the target body	Non-spherical mass distribution leads to interesting dynamics when an object is close.
Third body perturbation	Massive bodies	Gravitational attraction effect of large bodies that have a close passage.
Residual Dipole	Residual dipole on the spacecraft	Internal currents create dipoles that interact with the magnetic field of a body causing a torque.
Aerodynamic drag	Atmosphere	Friction between the satellite and the atmosphere. It depends on the altitude.
Albedo Pressure	The reflection of the Sun from the small body	Depends on the solar flux and on the latitude and longitude of the spacecraft.
Radiation Pressure	Temperature of the main body	Heat coming from the target body, usually assumed as black body radiation. For example, 400 Watts for the Earth.
Outgassing	Humidity in the structure	Provoked by the heating of surfaces, thus resulting in the emission of gases that can produce forces.
Radio Frequency (RF)	Transmit antennas	Radiation pressure obtained by diving the power and the speed of light.
Thermal Pressure	Radiators	Heat from radiators diffuses creating a thrust proportional to the heat flux.
Leaks	On-board gas and liquid supplies	Leaks act as type of cold gas thruster.
Thruster Plumes	Thruster system	Interaction between non-regular rocket exhaust plumes and the structure of the thruster.

Table 4: External disturbances that affect a spacecraft [7, 1].

As seen in the previous table, there is a moderately long list of disturbances affecting the spacecraft; although, due to various reasons, not every type of disturbance can or must be considered in this scenario. Some disturbances are associated solely to the asteroid system properties (or whichever celestial body is being observed), some others are associated only to the spacecraft characteristics and the rest of them happen because of the interaction between the spacecraft and the environment of asteroid. [7] The focus of this thesis is on the disturbances related to the space environment; therefore, only these are considered in this study. In the upcoming subsection, the relevant disturbances will be described.

Moreover, one should not forget about the internal disturbances of the spacecraft which cause jitter. Jitter refers to errors in the attitude of a spacecraft due to high frequencies that cannot be controlled by the ADCS because this system is inherently bounded to a controller period that determines the bandwidth at which the control system can operate correctly. These internal high-frequency disturbances can come from: rotating components with off-diagonal inertia terms, rotating and sliding parts such as motors, rotor imbalances, slosh of internal liquids and from structural deformation caused by rapid changes of temperature. [7]

5.4 Disturbance Modelling

In the case of small bodies, perturbations like the solar radiation pressure or the non-spherical shape become very significant. Additionally, there are other forces that also need to be considered, such as third body perturbations caused by the gravitational fields of large bodies that have a close passage. All of these disturbances need to be modelled in order to reproduce a more realistic representation of the motion. The disturbances can also be classified into gravitational and non-gravitational. The magnetic residual disturbance or the atmospheric drag are examples of the non-gravitational ones; although, in our system, the only significant non-gravitational disturbance is the solar radiation pressure. In general, the disturbance torque, ${}^S N_{ext}$, acting on the satellite can be determined as [51, 4, 1]:

$${}^S N_{ext} = {}^S N_G + {}^S N_R + {}^S N_E \quad (16)$$

where ${}^S N_G$ is the torque caused by gravitational forces, ${}^S N_R$ is the torque caused by the solar radiation and ${}^S N_E$ corresponds to other external torques as shown in Table 4. If required, these other external torques can potentially be added into the same equation. Since this thesis concerns mainly on the environment disturbances, we will set it to zero, ${}^S N_E = 0$. These other torques come from different sources. This equation is set in the (S) frame. In this section, these two main types of disturbances affecting the attitude of the satellite are described.

5.4.1 Gravitational Disturbances

The forces corresponding to the main gravitational disturbances are listed below.

- Asteroid spherical harmonics.

- Sun, Earth, Jupiter and Didymoon disturbances.
- Gravity gradient.

The first gravitational disturbance arises from the non-regular shape of the asteroid, entailing that its gravity field is not uniform. This quality affects the orientation and motion of the satellite. This model was already developed in chapter 4. The second disturbance is the gravitational attraction force of third bodies, such as the Sun, the Earth, Jupiter and the secondary of the asteroid will affect the orbit and attitude of the spacecraft. Lastly, the gravity gradient disturbance is caused by the non-spherical shape and non-uniform mass distribution of the spacecraft itself. It provokes a gravitational torque around its center of mass, mainly due to the gravitational force of the primary asteroid. [1, 25]

Third bodies

If it is assumed that the center of mass of the small body rests in a plane on a two-body orbit. Then, gravitational perturbations caused by the Sun or other planets are simple to determine. Under certain circumstances this works as a sufficiently accurate model, but it completely ignores more complex scenarios where simultaneous gravitational disturbances occur and there is no analytical solution. [52]

According to Newton's law of universal gravitation, the absolute gravitational attraction that a particle would experience is given by $-\left[(GM_p)/(|\mathbf{r} - \mathbf{d}|^3)\right](\mathbf{r} - \mathbf{d})$. Here, M_p corresponds to the mass of the perturbing body, \mathbf{r} is the vector from the small body center of mass to the particle and \mathbf{d} is the position vector from the small body center of mass to the perturbing body. In this case, the perturber is seen as an orbiter of the small body, which is just a matter of perspective, since the relative quantity is the important one. [1]

The absolute acceleration of a body is not used to find its motion relative to the small body. Instead, the difference between the acceleration of the particle of the small celestial body body is considered. It is defined as $+[(GM_p)/|\mathbf{d}|^3]\mathbf{d}$. Here, \mathbf{d} is the position vector of the perturbing body relative to the central body. The difference between these terms forms the perturbation gravitational acceleration, \mathbf{a}_p , from a body with mass M_p as [1]:

$$\mathbf{a}_p = -GM_p \left[\frac{(\mathbf{r} - \mathbf{d})}{|\mathbf{r} - \mathbf{d}|^3} + \frac{\mathbf{d}}{|\mathbf{d}|^3} \right]. \quad (17)$$

The terms of a perturbing acceleration potential, \mathbf{R}_p , are more useful in this analysis as [1]:

$$\mathbf{R}_p = GM_p \left[\frac{1}{|\mathbf{r} - \mathbf{d}|} - \frac{\mathbf{d} \cdot \mathbf{r}}{|\mathbf{d}|^3} \right], \quad (18)$$

where,

$$\mathbf{a}_p = \frac{\partial \mathbf{R}_p}{\partial \mathbf{r}}. \quad (19)$$

Moreover, if the distance between the central body and the perturbing body, d , is significantly larger than the distance of the particle from the central body ($d \gg r$), the perturbing potential can be expanded using the Legendre expansion as [53]:

$$\mathbf{R}_p = \frac{\mu_p}{d} \left[\sum_{i=0}^{\infty} \left(\frac{r}{d} \right)^i P_{i0}(\mathbf{r} \cdot \mathbf{d}/rd) - \frac{\mathbf{d} \cdot \mathbf{r}}{|\mathbf{d}|^2} \right]. \quad (20)$$

μ_p is the product of GM_p . From Appendix B, the Legendre polynomial $P_{10}(x) = x$ and $P_{00}(x) = 1$. This leads to a cancellation between the $i = 1$ term and the second term in the summation. The first term of the summation adds just a constant value and the perturbation terms that are important start at $i = 2$, resulting in the perturbation acceleration [1]:

$$\mathbf{R}_p = \frac{\mu_p}{d} \sum_{i=0}^{\infty} \left(\frac{r}{d} \right)^i P_{i0}(\mathbf{r} \cdot \mathbf{d}/rd). \quad (21)$$

Normally, when this expansion is used, only the first term is retained while neglecting the rest. Evaluating this term explicitly, with the Legendre polynomial $P_{20}(x) = \frac{1}{2}(3x^2 - 1)$. It yields [1]:

$$\mathbf{R}_p = \frac{1}{2} \frac{\mu_p}{d^3} \left[3(\mathbf{r} \cdot \hat{\mathbf{d}})^2 - r^2 \right]. \quad (22)$$

Here, $\hat{\mathbf{d}}$ is the normalised vector or unit vector of the non-zero vector \mathbf{d} . It is defined as

$$\hat{\mathbf{d}} = \frac{\mathbf{d}}{|\mathbf{d}|}, \quad (23)$$

where $|\mathbf{d}|$ is the norm of \mathbf{d} . It should be highlighted that the orientation of \mathbf{d} makes no difference in this form of perturbation. However, when it is combined with a rotating reference frame, it creates the tidal acceleration, which will not be discussed in this model. [34] Finally and in conclusion, when multiple bodies are attracting the spacecraft, a different perturbation potential can be defined for each case and summed at the end to calculate the full potential. This perturbation relies heavily on the position \mathbf{d} and it is time-varying. The position can be supplied by motion models or by the aforementioned ephemerides. [1]

Gravity Gradient

The gravity force between a spacecraft and another body, i.e. an asteroid, at a distance $\|R_{SA}\|$ from the center is:

$$|F| = G \frac{M_A m_{SA}}{\|R_{SA}\|^2}, \quad (24)$$

where m_{SA} is the mass of the spacecraft and M_A is the mass of the asteroid. However, this force is not the same for different parts of the satellite, because gravity force weakens with the distance from the surface. Thus, causing torques that affect the orientation of the satellite. Figure 19 illustrates this effect. Notice how force, F_1 is greater than force, F_2 , causing a counterclockwise torque around the center of mass of the satellite. [4] The equation can be written as [46]:

$${}^S N_{GG} = \frac{3\mu_p}{|{}^S R_{SA}|^3} \left[{}^S \hat{R}_{SA} \times \left({}^S I \cdot {}^S \hat{R}_{SA} \right) \right], \quad (25)$$

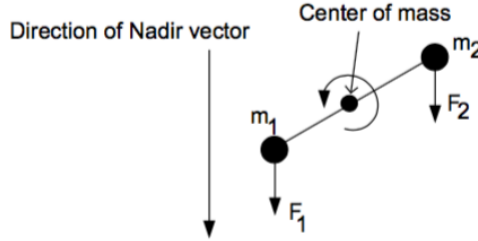


Figure 19: Illustration of the gravity gradient torque [4].

where ${}^S R_{SA}$ is the vector from the center of the asteroid to the spacecraft and ${}^S I$ is the moment of inertia, both in the (S) frame.

5.4.2 Solar Radiation Pressure

As mentioned in section 4, radiation coming from the Sun and hitting the surface of the satellite will cause an exchange of momentum that will be experienced as a torque around the center of mass of the spacecraft. Although there are some complex models describing this interaction, a simpler approach defining first the force, $|F_R|$, as in [46], will be used as follows:

$$|F_R| = KAP. \quad (26)$$

This magnitude depends on the momentum flux from the Sun, P , whose value is $4.4 \cdot 10^{-6} \text{ kg/ms}^2$. It is also proportional to the reflectivity factor or solar absorption coefficient K , which is a dimensionless constant value that depends on the material of the spacecraft's surface and it varies from 0 to 2. The lowest value corresponds to a completely transparent surface and the highest value means a full reflective material. Lastly, A is the illuminated cross-sectional area perpendicular to the vector that joins the spacecraft to the Sun. [46]

This force acts opposite to the direction of the vector from the satellite to the Sun. For this reason, a negative unit vector in the direction of ${}^I R_{SA \rightarrow S}$ is added to the last equation

$${}^I F_R = -KAP {}^I \hat{R}_{SA \rightarrow S}. \quad (27)$$

The disturbance torque can be then computed as a rotation of this force in the spacecraft reference frame and it is expressed as

$${}^S N_R = {}^S F_R \times {}^S R_{com}, \quad (28)$$

being ${}^S R_{com}$ the vector from the center of mass of the satellite to its geometrical center.

5.4.3 Total Disturbance Torque

The most important disturbances affecting the motion of the satellite have been detailed. The last step consists of writing the total perturbation in a single expression. It is the summation of the previous models:

$${}^S N_{ext} = {}^S N_{TBP} + {}^S N_{GG} + {}^S N_{AZH} + {}^S N_R \quad (29)$$

where, ${}^S N_{TBP}$ is the torque caused by third bodies. ${}^S N_{GG}$ is the disturbance torque due to the gravity gradient and ${}^S N_{AZH}$ is the torque caused by the non-spherical shape of the asteroid.

5.5 Orbit Propagator

As previously stated, the disturbance models depend on the position of the satellite. A model that describes the orbit of the satellite around the binary asteroid needs to be determined. Usually, when there is a significant mass difference between two bodies, the two-body approach can provide very accurate solutions. For example, the satellite, and/or moons, are treated as particles, or mass-less bodies, rotating a massive body and it works effectively in most of the astrodynamical problems. Nonetheless, this approximation presents shortcomings when it comes to a system where the gravitational field of a third body is still effective. [11] Like in the case of the ASPECT mission scenario.

A more precise solution to this type of astrodynamical problems would integrate four classical models found in astrodynamics. They are: the full two-body problem, the non-spherical orbiter, the Hill problem and the restricted three-body problem. However, this constitutes a more complex simulation challenge. The simplest way to model a binary asteroid for an initial design and analysis is referred as the Circular Restricted Three Body Problem (CR3BP). This model provides accurate results for binary systems in design phase. [11, 1, 54]

In this model, two massive bodies are rotating around their common center of mass according to Newton's or Kepler's laws. A third body, with a negligible mass and gravitational field, moves under the gravity influence of the first two bodies. In this particular mission, the two massive bodies are the primary and the secondary bodies of the asteroid system. The third body represents the satellite. [54]

Equations of Motion Circular Restricted Three Body Problem

In this section, the motion of a spacecraft is given according to the CR3BP. Figure 20 illustrates the CR3BP; the three bodies lie on a co-rotating frame around the barycentre of m_1 and m_2 , which are the massive bodies. The motion of m_1 and m_2 is circular about their common center of mass with angular speed ω [11]. It is expressed as

$$\omega = \frac{2\pi}{T}, \quad (30)$$

where T is the period of motion calculated from

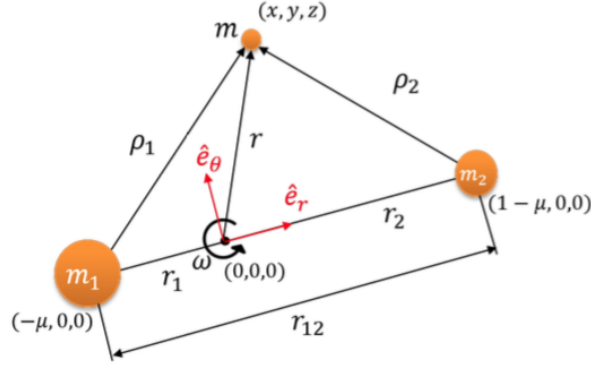


Figure 20: Circular restricted three body problem illustration [54].

$$T = 2\pi \sqrt{\frac{\mu}{r_{12}^3}}, \quad (31)$$

being μ the gravitational constant of the system; which is the total mass of the binary multiplied by the universal gravitational constant, $G(m_1 + m_2) = \mu_1 + \mu_2$ [54]. Next, the square of the magnitude of the angular velocity is:

$$\omega^2 = \frac{G(m_1 + m_2)}{r_{12}^3} = \frac{\mu_1 + \mu_2}{r_{12}^3}. \quad (32)$$

Further, the position of the spacecraft m , represented by r , can be written in terms of this rotating frame as

$$\mathbf{r} = r_x \hat{e}_r + r_y \hat{e}_\theta + r_z \hat{e}_3. \quad (33)$$

Afterwards, the acceleration must be defined, thus the derivative of \mathbf{r} to calculate the gravitational force acting on the spacecraft.

$$\mathbf{r} = (\ddot{r}_x - 2\dot{r}_y\omega - r_x\omega^2) \hat{e}_r + (\ddot{r}_y + 2\dot{r}_x\omega - r_y\omega^2) \hat{e}_\theta + \ddot{r}_z \hat{e}_3. \quad (34)$$

Force equals,

$$\mathbf{F} = \mathbf{F}_1 + \mathbf{F}_2 = - \left[\begin{array}{c} \frac{\mu_1(r_x + r_1)}{\rho_1^3} + \frac{\mu_2(r_x - r_2)}{\rho_2^3} \\ \left(\frac{\mu_1}{\rho_1^3} + \frac{\mu_2}{\rho_2^3} \right) r_y \\ \left(\frac{\mu_1}{\rho_1^3} + \frac{\mu_2}{\rho_2^3} \right) r_z \end{array} \right] \quad (35)$$

and the equations of motion are

$$\ddot{r}_x - 2\dot{r}_y\omega - r_x\omega^2 + \frac{\mu_1(r_x + r_1)}{\rho_1^3} + \frac{\mu_2(r_x - r_2)}{\rho_2^3} = 0, \quad (36)$$

$$\ddot{r}_y - 2\dot{r}_x\omega - r_y\omega^2 + \left(\frac{\mu_1}{\rho_1^3} + \frac{\mu_2}{\rho_2^3}\right)r_y = 0, \quad (37)$$

$$\ddot{r}_z + \left(\frac{\mu_1}{\rho_1^3} + \frac{\mu_2}{\rho_2^3}\right)r_z = 0. \quad (38)$$

Here, ρ_i represents the relative distance of m respect to m_i ,

$$\rho_{i=1,2} = \sqrt{(x - r_i)^2 + y^2 + z^2}. \quad (39)$$

Finally, with this set of equations, it is possible to describe the orbit of a spacecraft around the primary and the secondary bodies of the asteroid system.

5.6 Satellite Model

In this part, the description of the dynamic and kinematic equations governing the attitude of the spacecraft is provided. Choosing a simple and rigid body structure is adequate to make the task more easily. The system of equations are based on Newton's laws of motion and on Euler's laws of angular momentum. This is the common approach in [46, 37, 10, 55, 4, 1].

Kinematic model

The kinematic model in quaternion parameters, $\dot{\mathbf{q}}_{os}$, is [55]:

$$\dot{\mathbf{q}}_{os} = \frac{1}{2}\Omega_{os}\mathbf{q}_{os} \quad (40)$$

$$\Omega_{os} = \begin{bmatrix} 0 & \omega_z & -\omega_y & \omega_x \\ -\omega_z & 0 & \omega_x & \omega_y \\ \omega_y & -\omega_z & 0 & \omega_z \\ -\omega_x & -\omega_y & -\omega_z & 0 \end{bmatrix}, \quad (41)$$

where the matrix Ω_{os} contains the angular velocities ω_x , ω_y and ω_z . Together, they form the angular velocity vector ω_{os}^s about the axes of the (S) frame with respect to the (O) frame. The complete derivation is found in [46]. Furthermore, ω_{os}^s can be expressed in terms of the spacecraft's angular velocity in the inertial reference frame (I) and the angular velocity in the orbit frame (O), both respect to the body or satellite (S) as [51]

$$\omega_{is}^s = \omega_{io}^s + \omega_{os}^s. \quad (42)$$

From this last equation, ω_{os}^s can be written in the form

$$\omega_{os}^s = \omega_{is}^s - R_o^s \omega_{io}^o, \quad (43)$$

where R_o^s is the rotation matrix from the orbit reference frame (O) to the spacecraft reference frame (S). Moreover, by assuming a planar circular orbit the angular velocity becomes

$$\omega_{io}^o = \begin{bmatrix} 0 \\ -\omega_o \\ 0 \end{bmatrix}; \quad (44)$$

and finally, the rotation matrix R_o^s is computed in quaternions as follows [51]

$$R_o^s = \begin{bmatrix} q_1^2 - q_2^2 - q_3^2 + q_4^2 & 2(q_1q_2 + q_3q_4) & 2(q_1q_3 - q_2q_4) \\ 2(q_1q_2 - q_3q_4) & -q_1^2 + q_2^2 - q_3^2 + q_4^2 & 2(q_2q_3 + q_1q_4) \\ 2(q_1q_3 + q_2q_4) & 2(q_2q_3 - q_1q_4) & -q_1^2 - q_2^2 + q_3^2 + q_4^2 \end{bmatrix}. \quad (45)$$

Dynamic model

The Euler's moment equation for a rigid body is established as [51]

$$\mathbf{M} = \dot{h}_i^s = \dot{h}_s^s + \omega_{is}^s \times h_s^s. \quad (46)$$

It is important to notice that all the vectors are expressed in the (S) frame and that \dot{h}_s^{is} represents the change of angular momentum of the satellite, which can only come from external applied torques; for instance, disturbances or actuators. The first term of the above equation is the change of angular momentum seen from the (S) frame, whereas the second term is the change caused by the rotation of the rotation of the (S) frame itself respect to the inertial frame, (I). [55] Thereafter, considering Euler's moment equation and the angular momentum formula, $h = I\omega$; the following expression is defined:

$$\mathbf{T} = I\dot{\omega}_{is}^s + \omega_{is}^s \times I\omega_s^{is}. \quad (47)$$

Here, \mathbf{T} represents the applied external torques, actuators and disturbances; I is the moment of inertia matrix of the satellite in the controller reference frame (C) as it is easier to handle, because the inertia matrix would have zero values except in the main diagonal. Finally, the dynamic model can be expressed in the form of a system of first order differential equations;

$$\dot{\omega}_x = \frac{\omega_y\omega_z(I_y - I_z) + T_x}{I_x}, \quad (48)$$

$$\dot{\omega}_y = \frac{\omega_x\omega_z(I_z - I_x) + T_y}{I_y}, \quad (49)$$

$$\dot{\omega}_z = \frac{\omega_x\omega_y(I_x - I_y) + T_z}{I_z}. \quad (50)$$

This state space representation shows that the angular velocity has an interdependency between its elements due to the moments of inertia and the application of external torques [55]. In this thesis, only the disturbance torques shown in equation (29) are considered. Although, the inclusion of actuator models is an intended and feasible extension of the project, as well as the inclusion of other types of disturbances.

6 Simulation Environment

In the following sections, the detailed explanation of the model implementation is given. The LEO simulator, by Aalborg University, was configured and reprogrammed according to the models described in chapters 4 and 5. Ultimately, the output of the simulator consists of the external disturbances, which are necessary to compute during the design of the ADCS. Users should be able to perform satellite attitude control analysis and may be able to design control loops or estimators. The principal outer purpose is to select suitable sensors and actuators, as well as spacecraft parameters. This selection depends on the disturbances coming from the asteroid space environment. Moreover, this simulator should be able to be configured and adapted according to any new discoveries or data regarding the asteroid system or mission requirements. It is developed in a Matlab and SIMULINK environment and it exploits in a simple, but effective manner, the features that this numerical simulation environment provides. Libraries within this software offer a wide range of functions, useful for the purposes of implementing the models. For instance, the Robotics toolbox and the Aerospace toolbox permit to execute operations such as change of coordinate systems and calculation of ephemerides. Another feature is the facility to setup a user interface and to initialise variables. Also, simulation results can be conveniently manipulated and plotted.

6.1 Simulation Framework

The general structure of the simulator is shown in Figure 21. The architecture of the ASPECT simulator maintains the same structure of the Aalborg simulator. It is composed of four blocks: the orbit propagator, the ephemerides models, the spacecraft dynamic model and the environment disturbances models. At the same time, each block is constructed of several subsystems. Certain subsystems were completely modified, some were partially adjusted and others remained as in the LEO simulator. Each block processes specific information, which is described in the forthcoming sections. But before that, a clarification of how each block was customised, in comparison to the LEO simulator, is given below.

The orbit propagator has two subsystems: the time calculator and the orbit calculator. The first was partially modified to set the date boundaries of the ASPECT mission. The second was completely redefined. The ephemerides block was changed completely; with more simple, but equally effective functions. It was adjusted to the mission scenario by adding and removing the corresponding celestial bodies. On the other hand, the spacecraft dynamic model prevailed just as previously programmed, because it functions under the same principles of a rigid body. The environment disturbance block was partially modified. Many sources that affect a LEO satellite do not affect an asteroid. Thus, they were removed. Although, other were conserved and the pertinent modifications were done. The integration of these four blocks provides the disturbance torque and forces experienced by a satellite orbiting in the vicinity of the Didymos asteroid.

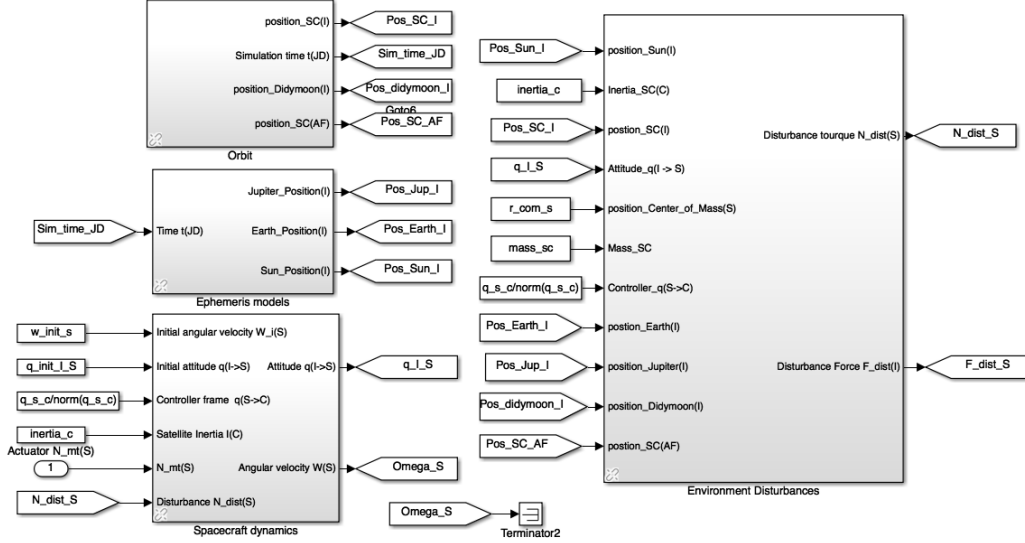


Figure 21: SIMULINK implementation of the asteroid space environment.

Time

Time is a fundamental dimension in all fields of science. In astrodynamics, time is critical, because objects move at high velocities. Numerical simulations performed by computers need a suitable implementation of time different from the conventional system of year/month/day. Therefore, a system denominated as Julian date (JD) was established. [56] In this system time is measured in days and its fractions since noon Universal Time on January 1, 4713 B.C. The next formula can be used to find the Julian date [57]:

$$JD = 367y - \text{floor} \left(\frac{7}{4} \left(y + \text{floor} \left(\frac{(m+9)}{12} \right) \right) \right) + \text{floor} \left(\frac{275m}{9} \right) + d + 1721013.5 + \frac{1}{24} \left(\frac{1}{60} \left(\frac{\text{sec}}{60} + \text{min} \right) + \text{hr} \right), \quad (51)$$

where y means year, m stands for month and d for day. The period of interest starts approximately at the beginning of July 2022 and finishes at the end of April 2023 as shown in Figure 11. These dates in Julian date format correspond to **2.4597615** and **2.4600645** respectively. These dates are established as the outermost boundaries of the simulator. The Figure 22 shows the configuration of the time subsystem. This subsystem is embedded in the orbit propagator block. Here, the initial date of the simulation is a preloaded variable, as well as the end date of the simulation. Both of them correspond to dates in Julian date format and they are chosen in the initial simulation setup (described in Appendix C). They serve as time limits of each simulation. At every step of the clock, the time is increased by one second

in the real system time. The duration of the simulation is chosen directly in the SIMULINK interface. Although, if the duration exceeds the selected end date, then it stops automatically. The simulation time is given to the ephemerides block and to the orbit propagator.

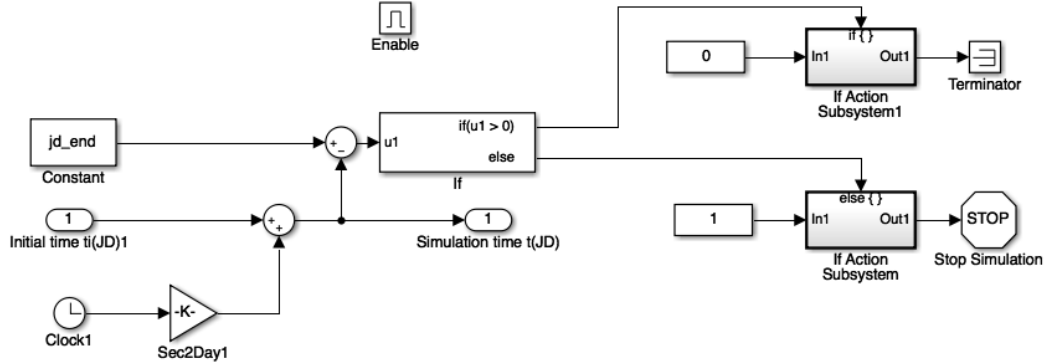


Figure 22: SIMULINK implementation of the simulation time.

6.2 Ephemerides Models

In this block, the positions of the Sun, the Earth and Jupiter in the asteroid reference frame (I) are calculated. The data of the relative position of the asteroid respect to the Sun is retrieved from the JPL's database. The information is extracted as a .csv file. Next, the file is imported to the Matlab workspace before running the simulation. The period loaded into the simulator comprehends from 28/06/2022 until 30/04/2023. The time precision is given in the order of minutes [43].

On the other hand, the Aerospace Toolbox provides the ephemerides of the Earth and Jupiter. Position and velocity of astronomical objects can be retrieved by a function denominated as 'planetEphemeris'. This function receives as arguments: the simulation time, a center body and a target body. The center and target bodies are restricted to the principal bodies of the Solar System. The data is calculated in a heliocentric reference frame. This information is given with a resolution of seconds. [58]

Lastly, a vector subtraction between the planets position and the asteroid position is done in order to switch from the Heliocentric reference frame to the asteroid inertial reference frame. The Figure 23 shows the SIMULINK integration. The input for the block is:

- the simulation time in Julian date format.

The output are:

- the position of the Sun in (I),

- the position of the Earth in (I),
- the position of Jupiter in (I).

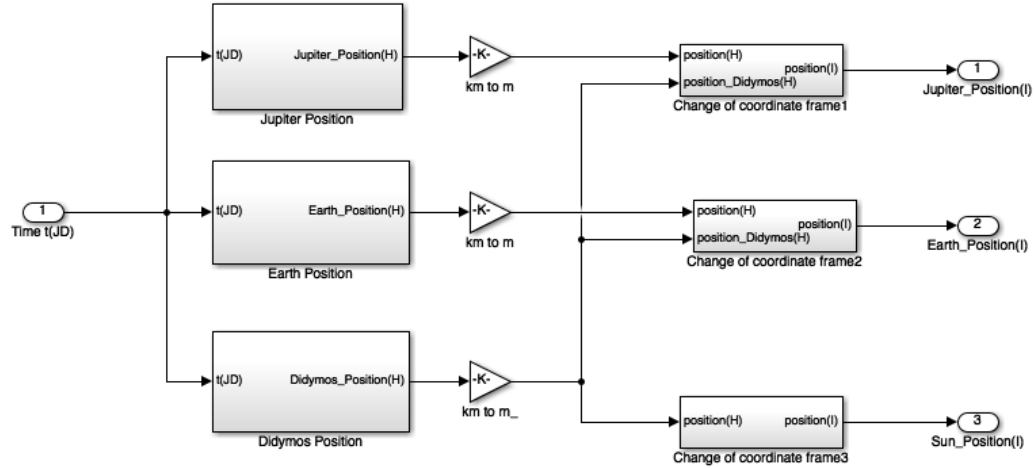


Figure 23: SIMULINK implementation of the ephemeris model.

6.3 Dynamic and Kinematic Models

The simulation of the motion of the satellite can be divided into two parts. The first part is the orbit propagator, which provides the movement of the satellite around the binary asteroid. This block is responsible for representing the local system containing the principal bodies: both bodies of the asteroid system and the spacecraft itself. The second part is the attitude simulation. Attitude refers to the angular position and rotational movement of the spacecraft due to internal and external torques. The torques are applied either by actuators or disturbances. These two modules describe the linear and rotational momentum of the spacecraft.

6.3.1 Orbit Propagator

In addition to the computation of the simulation time, the calculation of the spacecraft orbit with respect to the binary system is done in this block. The CR3BP model, described in section 5, is the appropriate approach for orbit determination and analysis of a binary system [1]. Nonetheless, this simulator is presently intended only for ADCS design. Hence, an optimal orbit control system is assumed. For this reason, an ideal circular orbit is implemented. The characteristics of this orbit are defined only by its radius; being 4.1 km the default value. Although, it can be changed as required for a different scenario. Likewise, Didymoon's orbit was implemented accordingly to [41]. In addition, the Robotics toolbox provides simple

rotation functions needed for coordinate transformations [59]. In particular, switching between the asteroid centered fixed reference frame and the asteroid inertial reference frame is required. The SIMULINK implementation is depicted in Figure 24. The input is:

- the initial time (JD).

The output are:

- the simulation time (JD),
- the position and velocity vectors of the secondary asteroid in (I),
- the position and velocity vectors of the spacecraft in (I),
- the position and velocity vectors of the spacecraft in (AF).

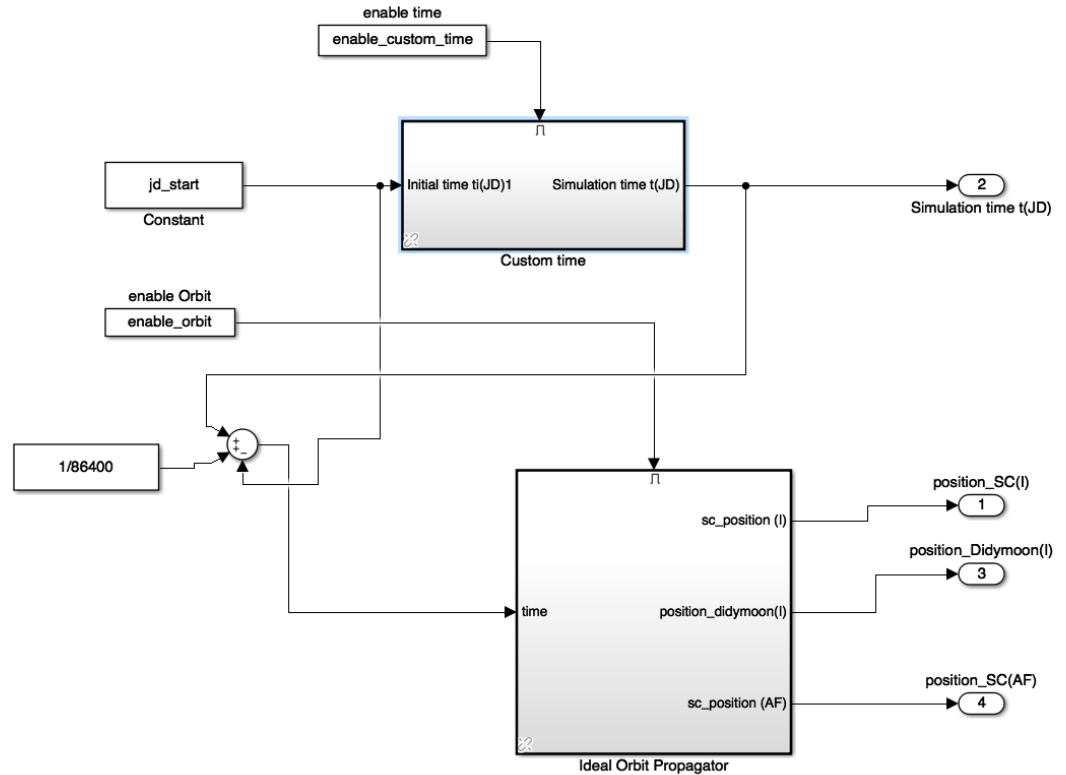


Figure 24: SIMULINK implementation of the orbit propagator.

6.3.2 Spacecraft Attitude

The model of the attitude of the spacecraft is shown in Figure 25. This block was entirely taken entirely from the LEO simulator. Inside it, pertinent rotations are made in quaternion form. The main functions implements the Euler's equations of angular momentum. The main part in this module is written in C to optimize the computation. Moreover, the input corresponding to the torque exerted by the actuators is set to zero, because no models of them have been developed yet for this project. However, this extension is feasible and would be compatible with the simulator. [4] The block needs two variable input:

- the torque of the actuators in (S),
- the external torque on the satellite due to disturbances in (S).

Besides, four constants are also required here: the initial values of the angular velocity, the initial attitude of the satellite, the inertia matrix in (C) and the rotation matrix to transform between the (C) and the (S) frames in quaternion form. [4] This block calculates two outputs:

- the angular velocity of the spacecraft in (S),
- the attitude of the satellite represented in quaternions.

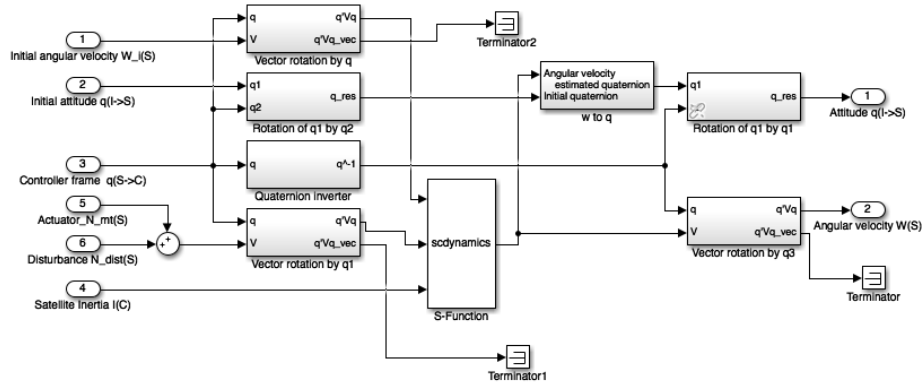


Figure 25: SIMULINK implementation of dynamics and kinematics of the satellite.

6.4 Environment Disturbances

The environment disturbance block is fed with all the information of the motion state of all the bodies of interest: the satellite, the Earth, the Sun, Didymoon and Jupiter. These are given in the proper reference frame according to the equations of each model. This block implements the environment disturbances models as follows:

- the gravitational perturbations:
 - gravity of the Sun.
 - gravity of the Earth.
 - gravity of Jupiter.
 - gravity of Didymoon.
 - gravity gradient.
 - asteroid zonal harmonics.
- the solar radiation pressure.

6.4.1 Third Body Perturbation

This block computes the disturbance associated to the gravity field of massive bodies pulling the ASPECT satellite. In principle, it performs the same operation as in the Aalborg simulator. The model works under the Newton's law of universal gravitation [4]. However, the bodies of interest are different. Naturally, the mass parameters that define this disturbance were adjusted accordingly. As seen in the list above, this model needs to be replicated four times as it considers: the Sun, the Earth, Jupiter and Didymoon. Also, the inertia and mass of the satellite are constants used in this block. An example of this model is shown in Figure 26, which corresponds to the Earth as the perturbing body. It works with two inputs, which are:

- the relative distance between the perturbing body and the satellite (I),
- the attitude of the satellite.

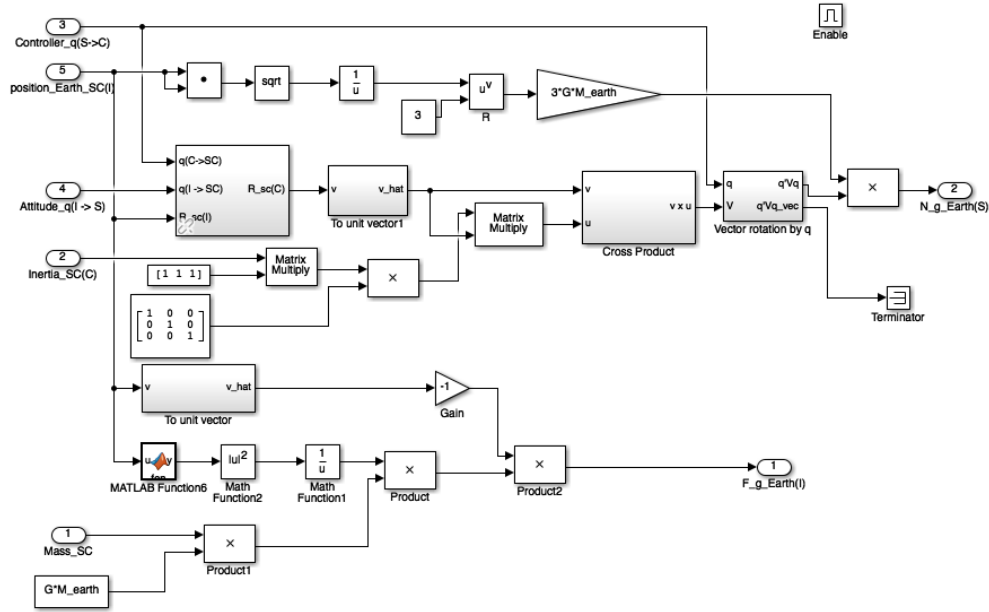


Figure 26: SIMULINK implementation of the third body disturbance with Earth as the perturbing body.

The outputs of the block are:

- the disturbance force in (I),
 - the generated torque in (S).

6.4.2 Gravity Gradient Model

The gravity gradient model holds the same structure as in the Aalborg simulator. Mass parameters obviously differ, but no other changes were made. This block considers the mass of the satellite, the mass of the primary body and the inertia of the spacecraft [4]. The model for the gravity gradient disturbance can be seen in Figure 27. It requires two inputs:

- a vector pointing from the center of the primary asteroid to the spacecraft in (S),
 - the attitude of the satellite.

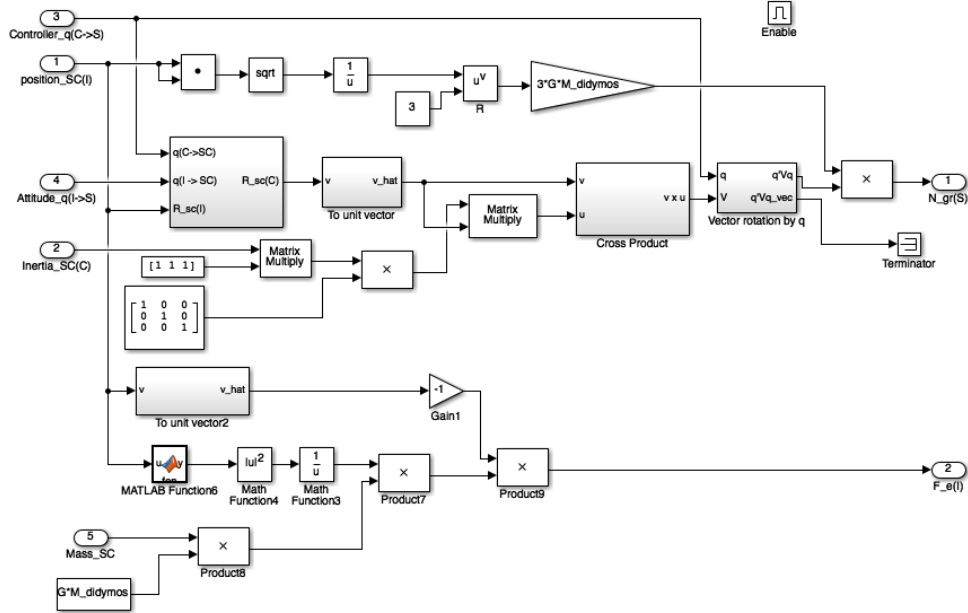


Figure 27: SIMULINK implementation of the gravity gradient disturbance.

The two outputs generated are:

- the gravity gradient torque in (S),
- the gravity gradient force in (I).

6.4.3 Asteroid Zonal Harmonics

This is the disturbance associated with the non-spherical shape of the asteroid. It depends on the zonal harmonic coefficients of the asteroid described in [42]. The Aalborg simulator contemplates the same type of disturbance. However, the central function was implemented distinctly. The Aerospace toolbox includes a function denominated as "gravityzonal". This function is used to make a zonal harmonic representation of gravity. One of the advantages of this function is that it permits a 'Custom' mode. If the oblateness (C20) and ellipticity (C22) coefficients of an astronomical body are known, the gravitational potential can be directly calculated up to second degree [58]. The function receives the following arguments: the position of the orbiter in (I); the degree of the harmonic model; the equatorial radius of the asteroid; the mass of the asteroid; and the zonal harmonic coefficients. The output of the function is a gravity vector in the x, y and z direction affecting the spacecraft. After, appropriate coordinate transformations are made. The SIMLUINK implementation is shown in Figure 28. The inputs are:

- the position of the satellite in (I),

- the attitude of the satellite.

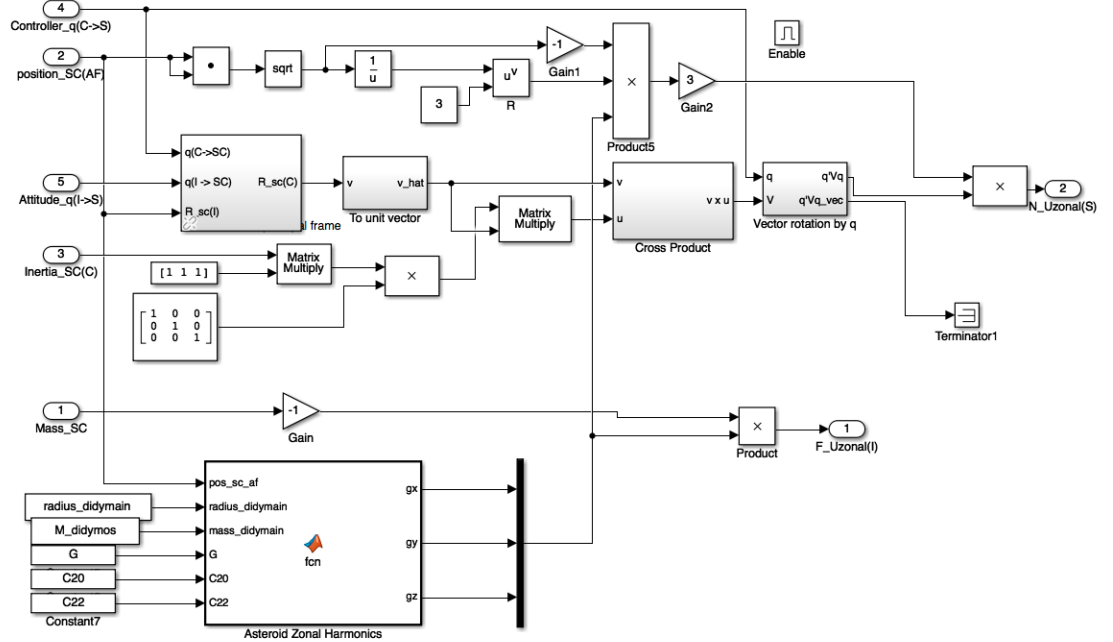


Figure 28: SIMULINK implementation of the asteroid zonal harmonics model.

The block computes two outputs:

- the disturbance torque in (S),
- the disturbance force in (I).

6.4.4 Solar Radiation Model

This disturbance can be calculated with the same approach in both simulators. It is a simple SRP model, but it provides an acceptable estimation [4, 1]. Therefore, the solar radiation model remains unmodified as compared to the Aalborg simulator. Here, the attitude is important not only to compute the torque experienced in the (S) frame, but also to calculate the exposed area as seen from the perspective from the Sun. This area corresponds to the cross-sectional area in equation 27. The model is depicted in Figure 29. [4] Three variable inputs are required:

- the attitude of the satellite,
- the position of the Sun in (I),
- the position of the Satellite in (I).

Next, two outputs are generated:

- the disturbance torque in (S),
- the disturbance force in (I).

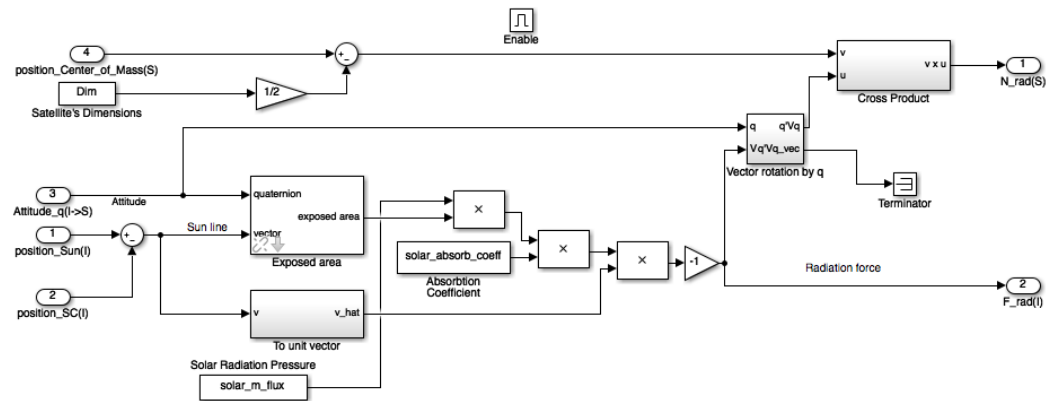


Figure 29: SIMULINK implementation of the solar radiation pressure model.

6.5 Masks: Constants and Parameters

A fundamental aspect of the simulator is the collection of all the constants and parameters required to characterise all the models used in the system. For example: the mass of the celestial bodies, the solar momentum flux, the dimension of the satellite, the initial attitude and other values that remain unchangeable during the simulation, but that are required to perform it. In SIMULINK, this is possible by creating a subsystem mask. This mask contains all the set-up information and it can also be easily modified according to the requirements in order to study the effect of different conditions. For example, one can study the effect of changing the location of the center of mass of the satellite on the attitude; or the effect of having a different orbit radius. The disturbance sources, which would be considered in the simulation, can also be selected. These parameters or properties are defined to characterise the ASPECT satellite, the Didymos asteroid system, the ideal circular orbit and the environment disturbances. Table 5 lists these four categories. The shown values of each parameter are set accordingly to the information given in previous sections, but they can be modified at convenience.

ASPECT Satellite	
Mass of the Satellite [kg]	4.5
Dimensions [x,y,z][m]	[0.3405,0.1,0.1]
Inertia Matrix of the Satellite [kgm^2]	[0.0075,0.0472,0.0472]
Center of Mass [x,y,z][m]	[0.0, 0.0, 0.0]
Controller Reference Frame (S->C)	[0 0 0 1]
Initial Attitude (I->S)[quaternion]	[0 0 0 1]
Initial Angular Rate (S)[rad/s]	[0 0 0]*0.2*(pi/180)
Solar Absorption Coefficient [-]	1
Didymos System	
Didymain mass [kg]	5.24e11
Didymoon mass [kg]	3.45e9
Raidus Didymain [m]	385
Didymoon orbit raidus [m]	1056.2
Didymain spin period [sec]	2.259*60*60
Gravity Field Harmonic Coefficient C20	-0.023
Gravity Field Harmonic Coefficient C22	-0.0013
Ideal Circular Orbit Parameters	
Spacecraft orbit radius [m]	4100
X axis SC orbit inclination [°]	15
Y axis SC orbit inclination [°]	0
Z axis SC orbit inclination [°]	0
SC start orbit angle [°]	180
X axis Didymoon orbit inclination [°]	0
Y axis Didymoon orbit inclination [°]	0
Z axis Didymoon orbit inclination [°]	0
Enable Custom Time	✓
Enable Orbit Propagator	✓
Environment Disturbances	
Gravitational Constant [$\text{m}^3/(\text{kgs}^2)$]	6.67408e-11
Solar Momentum Flux [kg/(ms ²)]	4.5565e-6
Mass of the Sun [kg]	4.37e30
Mass of the Earth [kg]	5.9742e24
Mass of Jupiter [kg]	1.898e27
Enable Radiation Disturbances	✓
Enable Gravity Disturbances	✓
Enable the Gravity of the Earth	✓
Enable the Gravity of Jupiter	✓
Enable the Gravity of the Sun	✓
Enable the Gravity of Didymoon	✓
Enable Torque From Gravity	✓
Enable the Asteroid Zonal Harmonics	✓

Table 5: Mask parameters and constants used in the simulator.

7 Simulator Testing and Functional Verification

The simulator works as a tool to develop the ADCS of the ASPECT CubeSat. Now, it is possible to test the simulator under different mission setups. The section below describes an insight about the output information that the simulation environment can provide. It shows the behaviour of the different torque disturbances over time according to its configured parameters. Next, a set of demonstration cases representing different potential mission scenarios are performed to make a disturbance analysis. The objective is to identify which are the most significant disturbances and what is the order of magnitude of each one. The analyses that can be done with this simulator are fundamental for the beginning design phase.

7.1 Simulation Exemplification

An initial setup of the simulator environment must be done before running a simulation. This setup consists of loading specific data and choosing the parameters that will be evaluated. The explanation of how to use the simulator is given in Appendix C. The final purpose is to compare how the disturbances would change when varying the mask parameters of Table 5. These parameters are conditions which can be controlled or chosen. Although, in this exemplification, the default values are set according to the same table. Moreover, the loaded date corresponds to the beginning of October 2022 when the average distance from the Sun to the asteroid is 1.5AU. The plots of the results are shown as a cluster of graphs grouped in Figure 30. The torque contribution of each disturbance source is shown. The maximum torque and the average torque are highlighted in order to identify more easily which disturbances are more important to consider.

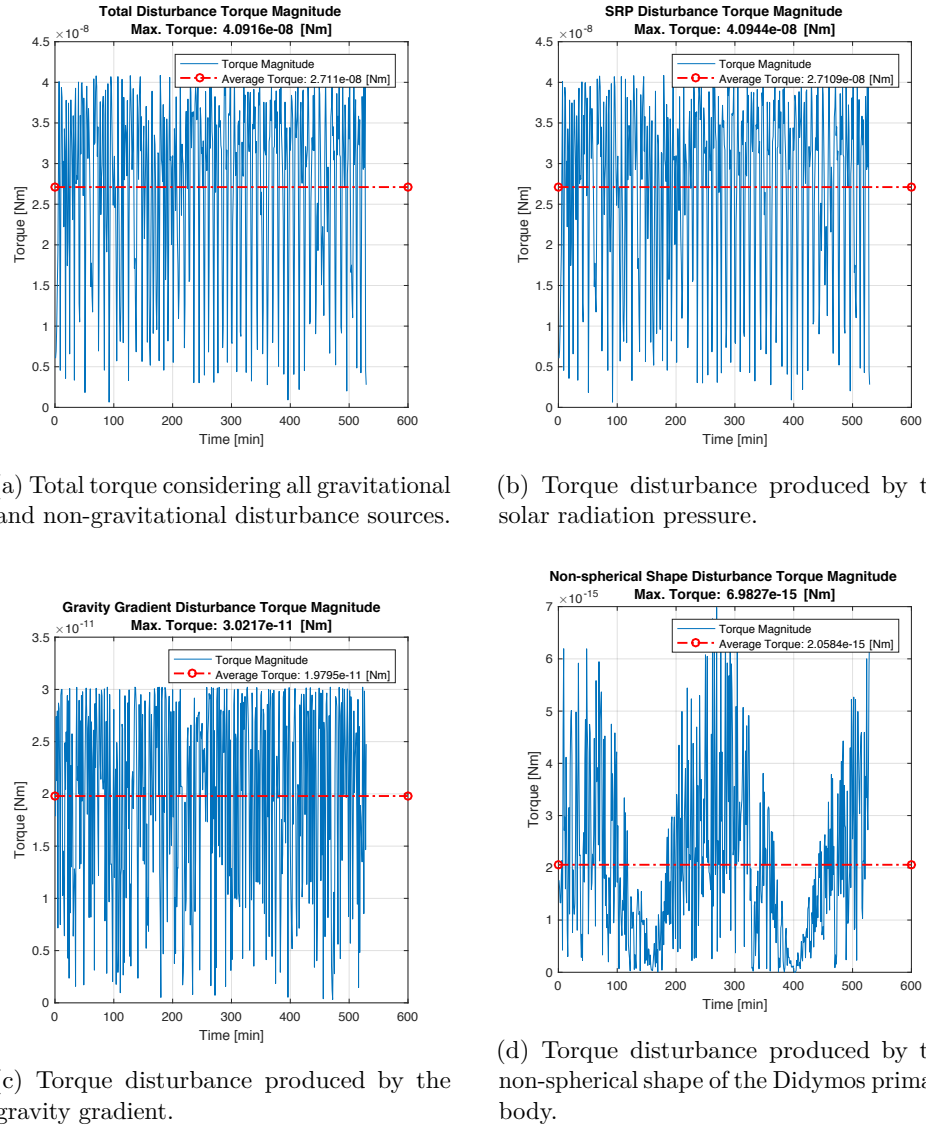


Figure 30: Magnitude of the disturbance torques produced by the different sources.

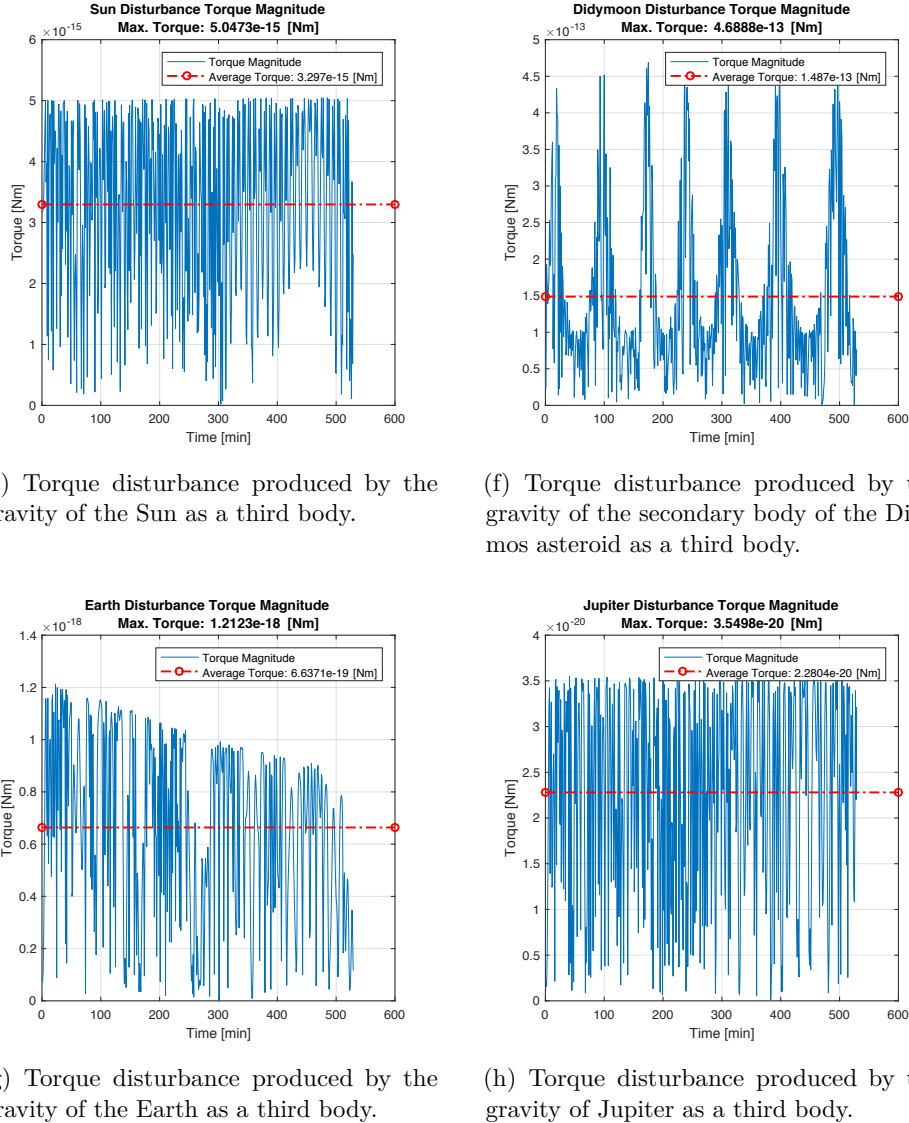


Figure 30: Magnitude of the disturbance torques produced by the different sources.

The time of the simulation considers a short span of approximately half a day. The plots shown in the Figure above evidently portrays the behaviour over time of each disturbance. The periodicity of the orbital motion can be clearly seen in the non-spherical shape disturbance and in the gravity disturbance caused by Didymoon. The peaks of the non-spherical shape correlate with the close passage between the satellite and Didymoon. Equally, the spherical harmonics model peaks when the satellite orbits at a point that is the closest to being collinear with the asteroid most elongated axis.

Further, as the mission progresses, the distances between the spacecraft and third bodies, such as the Earth, the Sun and Jupiter, increase. The Figure 30g shows this event, where the torque tends to the decrease. The same could be seen in the Sun and Jupiter disturbance cases if the time span of the simulation was markedly longer. Nonetheless, a short simulation period is one of the limitations of this environment. It can be overcome by performing and comparing two well separated dates of simulation as it is described in the next section.

7.2 Demonstration Cases

In this section the results and analysis of specific demonstration cases are portrayed. The purpose is to identify and quantify which are the most significant disturbances that would act on the ASPECT satellite. The relative distance between the spacecraft and the source of disturbance is elemental in every disturbance model. In particular, the distance to the Sun is crucial because it is the main source of both gravitational and non-gravitational disturbances. Further, the distance between the satellite and the asteroid system is important as well. For these reasons, six different demo cases were simulated.

These demo cases, or mission scenarios, result from simulating the maximum and the minimum distance to the Sun during the mission; and from setting 3 different circular orbit radii of the satellite. The Figure 31 presents the orbit of the asteroid, in a heliocentric perspective, corresponding to the expected period of the mission. It shows that the maximum distance is 1.8 AU whereas the minimum distance is 1 AU. These trajectories and their corresponding date periods are shown in Figure 32 and in Figure 33 respectively. On the other hand, three orbit radii were set in the simulator: the ideal expected orbit (4.1 km), an orbit deviated closer to the asteroid (1.2 km) and an orbit deviated further away from the asteroid (6.1 km). These orbits are depicted in Figure 35.

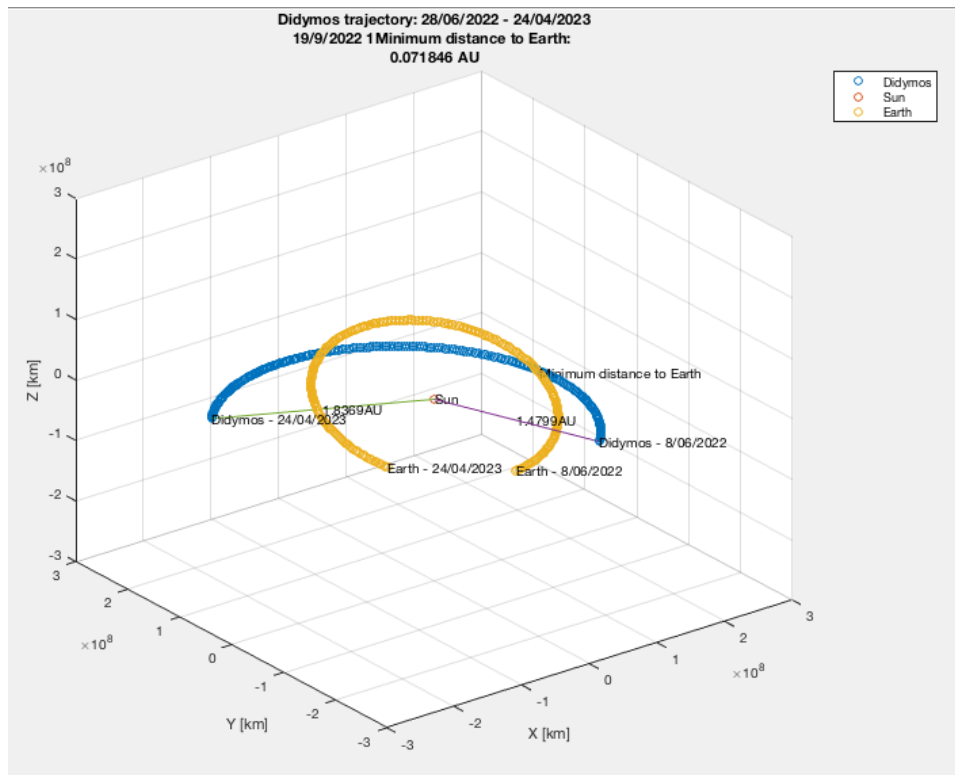


Figure 31: Didymos ephemeris 28/06/2022 - 24/04/2023. Maximum and minimum distances between the Sun and the asteroid/satellite system are 1 AU and 1.8 AU.

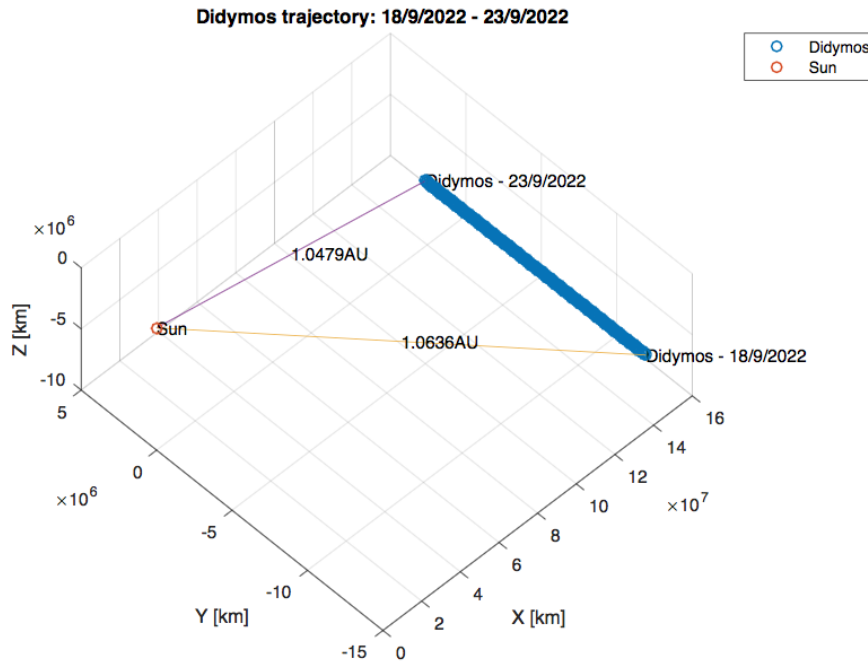


Figure 32: Didymos trajectory 18/September/2022 - 23/September/2022.

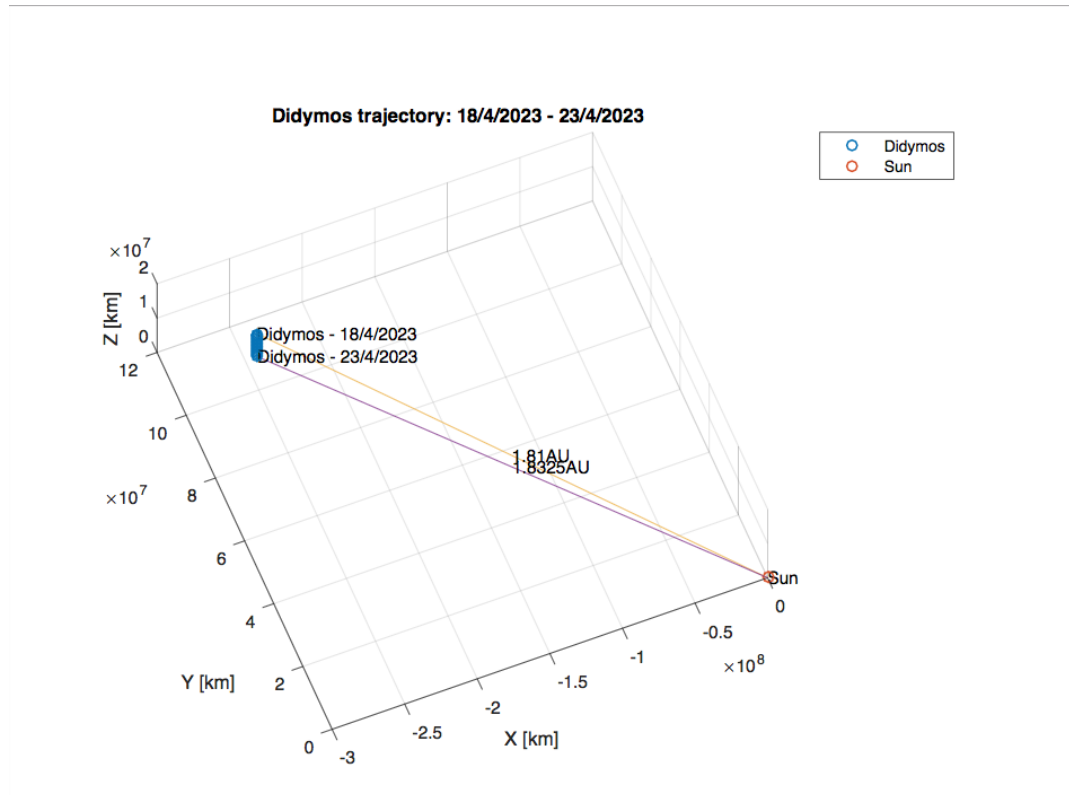


Figure 33: Didymos trajectory 18/April/2023 - 23/April/2023.

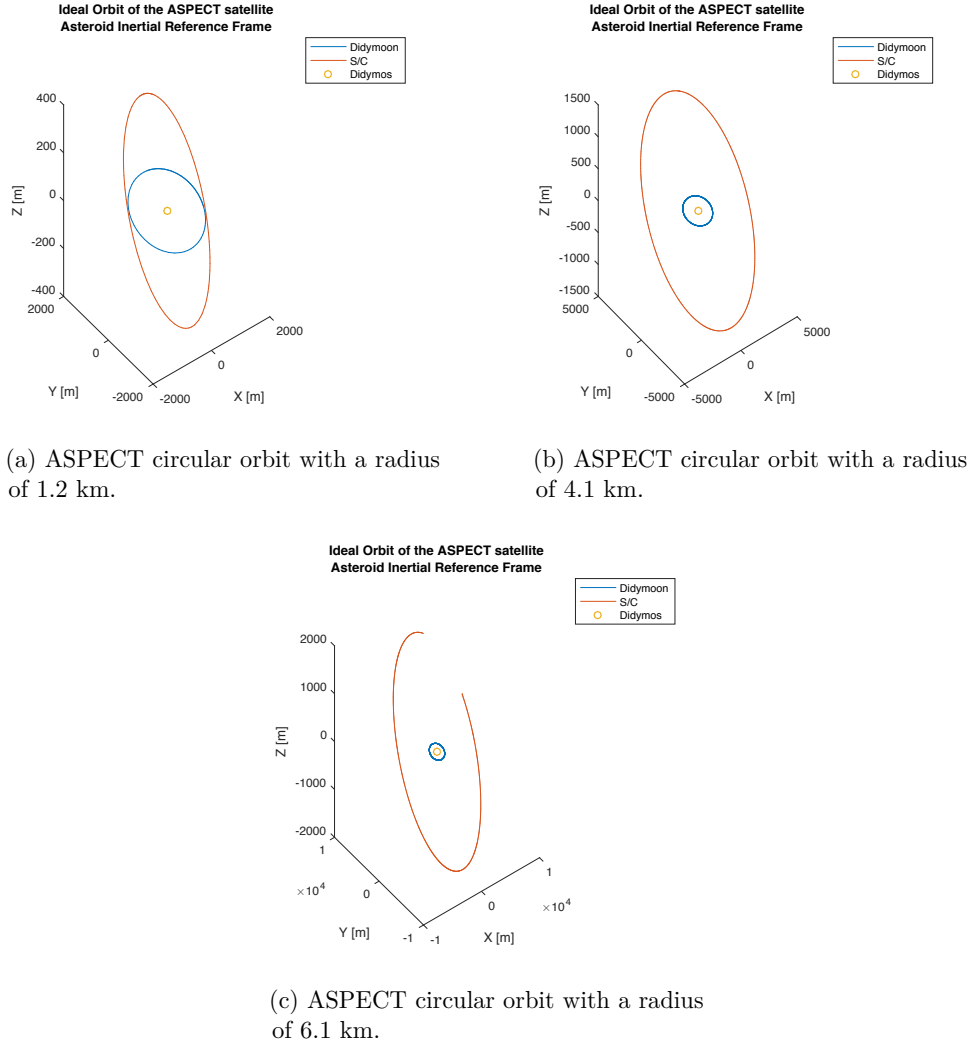


Figure 34: ASPECT satellite orbit motion in the asteroid fixed reference frame at different radii.

The simulator was set according to Table 5 with the exception of the orbit radius, which was modified at each simulation. The Table 6 shows the results of the torque disturbances at a distance of 1 AU. All the disturbance sources are listed with their corresponding contribution to the total torque. Next, the same results, but at 1.8 AU from the Sun, are presented in Table 7.

Distance to the Sun	1 AU		
Radius of the satellite orbit	1.2 km	4.1 km	6.1 km
Solar Radiation Pressure [Nm]	2.3093e-08	2.489e-08	2.5572e-08
Gravity Gradient [Nm]	7.9654e-10	2.1106e-11	6.145e-12
Non-spherical shape [Nm]	2.9769e-13	1.9629e-15	4.306e-16
Gravity of Didymoon [Nm]	4.2771e-11	1.5811e-13	4.3041e-14
Gravity of the Sun [Nm]	2.9206e-15	3.0181e-15	2.8324e-15
Gravity of the Earth [Nm]	2.0776e-17	1.7356e-17	1.6362e-17
Gravity of Jupiter [Nm]	2.5283e-20	2.6087e-20	2.431e-20
Total Torque [Nm]	2.39326e-08	2.49113e-08	2.55782e-08

Table 6: Environment disturbances torque magnitudes acting on the spacecraft at 1 AU from the Sun.

Distance to the Sun	1.8 AU		
Radius of the satellite orbit	1.2 km	4.1 km	6.1 km
Solar Radiation Pressure [Nm]	9.4648e-09	9.5934e-09	8.1262e-09
Gravity Gradient [Nm]	7.7756e-10	2.0507e-11	6.5458e-12
Non-spherical shape [Nm]	2.5366e-13	2.0821e-15	4.2419e-16
Gravity of Didymoon [Nm]	3.9358e-11	1.5693e-13	4.6701e-14
Gravity of the Sun [Nm]	6.4152e-16	6.4402e-16	5.9834e-16
Gravity of the Earth [Nm]	2.1698e-21	2.0379e-21	2.0414e-21
Gravity of Jupiter [Nm]	7.2026e-21	6.935e-21	7.1067e-21
Total Torque [Nm]	1.02820e-08	9.61407e-09	8.13279e-09

Table 7: Environment disturbances torque magnitudes acting on the spacecraft at 1.8 AU from the Sun.

The outcome of the simulations revealed interesting insights about the disturbance sources. Based on the values shown in Tables 6 and 7; overall, the maximum total disturbance torque is 25.5782 nNm and the minimum disturbance torque is 8.13279 nNm. However, the solar radiatlon pressure (SRP) constituted over the 99.9% of the total disturbance torque experienced by the ASPECT satellite in both cases. The clearest conclusion is that the solar radiation pressure exerts the strongest disturbance on the spacecraft. The second strongest torque comes from the gravity gradient disturbance, but it is at least one order of magnitude weaker than the torque applied by the SRP. At its strongest, it represented 7.56% of the disturbance torque, while the SRP had over 90%. This situation occurred when the spacecraft was 1.8 AU away from the Sun and 1.2 km away from the primary body of the asteroid.

Besides the former perturbations, the non-spherical shape disturbance and the gravity force of Didymoon applied the next significant torques on the spacecraft. However, these minor torques lack the impact of the non-gravitational source. Moreover, the incorporation of the gravitational pull force applied by third bodies such as the Earth, Jupiter and the Sun; represent practically a zero value. This does

not mean that these sources are not relevant. The awareness of their contribution is the important aspect. Nevertheless, given the circumstances of the mission, certain disturbances sources are not highly decisive when proposing an ADCS for this particular system.

7.3 Solar Absorption Coefficient

Once the SRP was defined as the strongest disturbance, in this section it is exemplified how it would be possible to mitigate its effect. The force of this perturbation, according to its current model, depends on four factors: the area exposed to the Sun, the solar momentum flux, the relative position between the Sun and the spacecraft and the solar absorption coefficient. From these parameters, the shape of the satellite and the material, thus solar absorption coefficient, are not particularly constrained by the mission scenario. By changing one or both factors, it is possible to alter the SRP disturbance torque.

The satellite flight model is still in concept design [5]. Hence, the shape is not finally defined and will certainly be modified along the development of the mission. On the contrary, the solar radiation coefficient could potentially be changed more easily. Two simulations are run with default parameters at 1 AU distance from the Sun, but with different coefficients: 0.1 and 1.9. The output of the tests are shown in Figure 35a for the low absorption coefficient and in Figure 35b for the high absorption coefficient.

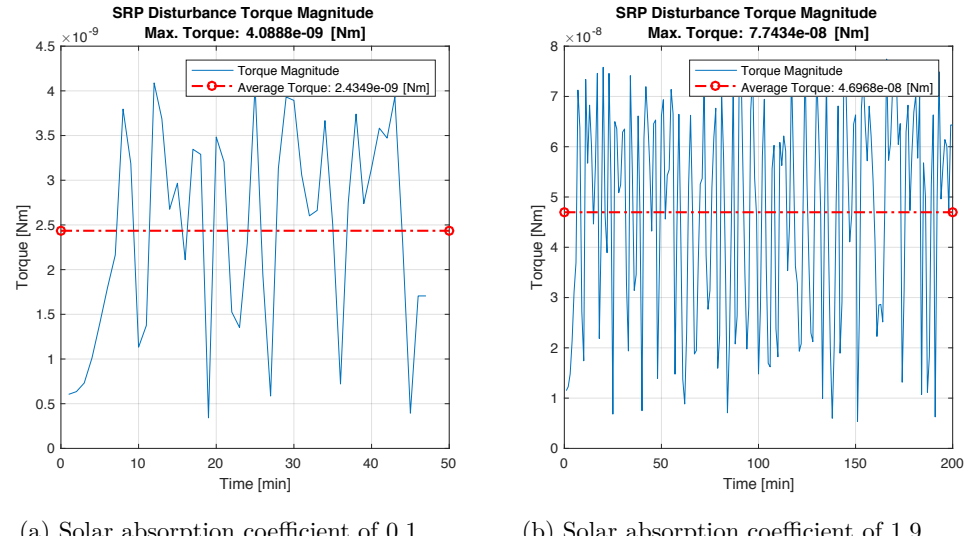


Figure 35: Solar Radiation Pressure torque magnitude acting on the ASPECT satellite according to different solar absorption coefficients.

The simulator computed a maximum of 4.09 nNm with an average of 2.43 nNm for the case of a low absorption coefficient. A maximum of 77 nNm and an average of 46.96

nNm were calculated when a 1.9 absorption coefficient was chosen. Undoubtedly, a significant change of the disturbance occurred; however, it does not alter the conclusions of the past section. Despite, the change of this coefficient, the solar radiation pressure remains as the most substantial disturbance in the analysis. This result is foreseen, since this proportional parameter ranges from 0 to 2; meaning that the order of magnitude would not be heavily modified. This test was exclusively a demonstration of how the simulator can be used to adjust and update the satellite parameters. Like this experiment, other setting of parameters or orbit scenarios can be performed to find an ideal configuration or a more precise determination of the ADCS.

8 Summary of Findings

The properties of the Didymos asteroid and the ASPECT mission were defined according to the latest studies and analyses. Didymos is an asteroid system with two bodies of 780 m and 163 m of mean radii respectively and it is presumably in a uniform rotation state. Its dynamic state is not fully constrained, but the information obtained through optical and radar observations is valuable enough to define mathematical models of the dynamics and kinematics of a satellite in its surroundings. The models include the gravitational and non-gravitational disturbance sources present in an asteroid environment.

The simulation of the models is paramount to design the ADCS of the ASPECT satellite. These models were implemented in a flexible software platform which was developed with Matlab and SIMULINK. The simulator is based on the architecture of a preceding LEO CubeSat project and it was adapted to the ASPECT mission scenario. The simulation shows the behaviour of the disturbance torques acting on the spacecraft. The objective was to identify the importance of each disturbance source and to quantify their effect. Further, this simulator can be easily adapted according to new findings about the asteroid or the requirements of the mission. Each simulation is characterized by certain parameters and initial setups, that can be chosen, regarding the CubeSat and the asteroid environment.

Various demonstration cases were simulated to verify and assess the functionality of this software tool. In these simulation cases, different orbit radii of the satellite in combination with the maximum and minimum distance between the asteroid and the Sun were tested. The average total torque disturbance is estimated to be in the order of nNm with an estimated maximum upper limit of not more than 100 nNm. Furthermore, the computation of the disturbances in every scenario revealed that the solar radiation pressure applies the strongest disturbance on the spacecraft. It represents above the 90% of the total disturbance torque. The SRP is followed by the local gravitational forces produced by the primary and the secondary bodies of the asteroid system: the non-spherical shape disturbance, the gravity gradient and the gravity of the secondary body. A last simulation case was performed in order to show how some spacecraft parameters can be changed to manipulate the effect of the disturbances.

8.1 Further Work

Some suggestions to improve the simulator are derived from the research and results obtained. The simulator is an early design platform which can be upgraded in several manners. For example, by testing different approaches or models to characterize the environment, which may be more realistic. A different determination of the gravitational potential or alternative models for the solar radiation pressure could be evaluated. Nonetheless, some models would require more specific information about the asteroid system or the satellite. Besides, the two major inclusions to the simulator should be done: the attitude and orbit motion coupling; and the sensor and actuators modelling. The design of ADCS considers the full behaviour of the

attitude of a satellite in space. Consequently, sensors and actuators need to be modelled and included. For instance, a gyroscope to measure the rotational state of the spacecraft or a star tracker to know the orientation respect to the Sun or other stars. In addition, actuators such as momentum wheels can be modelled and added to Equation 16. Momentum wheels can load and unload angular momentum and they are used for fast and small changes in attitude. However with this system, magnetorquers are required to desaturate the wheels. [4] In conclusion, small celestial bodies present unique properties that should be precisely determined with pertinent observations. Improvement of the asteroid, the disturbances and CubeSat models are fundamental to increase the opportunities and exploration capabilities of this interplanetary mission.

References

- [1] D. J. Scheeres, *Orbital Motion in Strongly Perturbed Environments: Applications to Asteroid, Comet and Planetary Satellite Orbiters.* Berlin: Springer, 2012.
- [2] ESA. (1999) Rosetta. Accessed 11/09/2016. [Online]. Available: http://www.esa.int/Our_Activities/Space_Science/Rosetta
- [3] A. Galvez, I. Carnelli, M. Fontaine, and C. Corral Van Damme, “Asteroid impact mission (AIM) & deflection assessment: an opportunity to understand impact dynamics and modelling,” in *Proceedings of the European Planetary Science Congress*, 2012.
- [4] D. Bhanderi, B. Andresen, C. Grøo, R. Hviid, C. Nielsen, K. Kresten, and D. Taagaard, “Attitude control system for aausat-2,” Aalborg University - Institute of Electronic Systems, Tech. Rep., 2005.
- [5] A. Näsilä, “Asteroid Spectral Imaging Mission,” ASPECT Project Report, 2016.
- [6] MultiMedia LLC. (2016) Attitude and Orbit Control System: Distributed Simulator. Accessed 17/04/2016. [Online]. Available: <https://fenix.tecnico.ulisboa.pt/downloadFile/395137455883/resumo.pdf>
- [7] M. Paluszek, S. Thomnas, J. Mueller, P. Bhatta, and P. Griesemer, *Attitude and Orbit Control Using the Spacecraft Control Toolbox V4.6.* Princeton Satellite Systems, 2008.
- [8] NASA. (2016) Spacecraft Navigation. Accessed 16/09/2016. [Online]. Available: <https://solarsystem.nasa.gov/basics/bsf13-1.php>
- [9] Jet Propulsion Laboratory. (2016) Deep Space Navigation. Accessed 16/08/2016. [Online]. Available: <https://scienceandtechnology.jpl.nasa.gov/research/research-topics-list/communications-computing-software/deep-space-navigation>
- [10] A. Misra and Y. Panchenko, “Attitude dynamics of satellites orbiting an asteroid,” *The Journal of the Astronautical Sciences*, vol. 54, no. 3, pp. 369–381, 2006.
- [11] O. Çelic, “Orbital environment considerations during close approach phase of missions to small bodies,” Master’s thesis, Cranfield University - School of Aerospace, Transport and Manufacturing, UK, 2015.
- [12] Space Flight System and NASA. (2016) Legacy and New LTTT Suite Optimization Tools. Accessed 16/09/2016. [Online]. Available: <https://spaceflightsystems.grc.nasa.gov/SSPO/ISPTProg/LTTT/>
- [13] Tech Briefs Media Group. (2016) Mission analysis, operations, and navigation toolkit environment (MONTE) version 040. Accessed 16/10/2016. [Online]. Available: <https://solarsystem.nasa.gov/basics/bsf13-1.php>

- [14] NASA. (2016) Near Earth Object Program. Accessed 17/03/2016. [Online]. Available: <http://neo.jpl.nasa.gov/neo/>
- [15] D. Garcia Yarnoz, J. Sanchez Cuartielles, and C. McInnes, "Applications of solar radiation pressure dominated highly non-keplerian trajectories around minor bodies," in *64th International Astronautical Congress*, 2013.
- [16] C. Murray and S. Dermott, *Solar system dynamics*. UK: Cambridge University press, 1999.
- [17] C. Peebles, *Asteroids: a history*. Smithsonian Institution, 2016.
- [18] D. Andrews, K. Bonner, A. Butterworth, H. Calvert, B. Dagang, K. Dimond, L. Eckeneroth, J. Erickson, B. Gilbertson, and N. Gompertz, "Defining a successful commercial asteroid mining program," *Acta Astronautica*, vol. 108, pp. 106–118, 2015.
- [19] Deep Space Industries. (2016) About Deep Space Industries. Accessed 15/01/2016. [Online]. Available: <http://deepspaceindustries.com/business/>
- [20] P. Sanchez, C. Colombo, M. Vasile, and G. Radice, "Multicriteria comparison among several mitigation strategies for dangerous near-earth objects," *Journal of Guidance, Control, and Dynamics*, vol. 32, no. 1, pp. 121–142, 2009.
- [21] NASA. (2016) Near-Earth Asteroid Rendezvous. Accessed 16/08/2016. [Online]. Available: <http://neo.jpl.nasa.gov/missions/near.html>
- [22] H. Demura, S. Kobayashi, E. Nemoto, N. Matsumoto, M. Furuya, A. Yukishita, N. Muranaka, H. Morita, K. Shirakawa, and M. Maruya, "Pole and global shape of 25143 Itokawa," *Science*, vol. 312, no. 5778, pp. 1347–1349, 2006.
- [23] JAXA. (2016) Asteroid Explorer "Hayabusa2". Accessed 18/09/2016. [Online]. Available: <http://global.jaxa.jp/projects/sat/hayabusa2/index.html>
- [24] NASA. (2016) Osiris REX - Asteroid Sample Return Mission. Accessed 08/09/2016. [Online]. Available: <https://www.nasa.gov/subject/6880/bennu/>
- [25] ESA. (2016) Asteroid Impact & Deflection Assessment mission. Accessed 15/01/2016. [Online]. Available: http://www.esa.int/Our_Activities/Space_Engineering_Technology/Asteroid_Impact_Mission/Asteroid_Impact_Deflection_Assessment_mission
- [26] ESA. (2016) Giotto. Accessed 10/09/2016. [Online]. Available: <http://sci.esa.int/giotto/>
- [27] S. Bhaskaran, *Autonomous navigation for deep space missions*. California: Jet Propulsion Laboratory and NASA, 2006.
- [28] NASA. (2016) Mars Reconnaissance Orbiter. Accessed 14/09/2016. [Online]. Available: <http://mars.nasa.gov/mro/mission/spaceship/parts/gnc/>

- [29] NASA. (2016) Asteroid Impact and Deflection Assessment (AIDA) Mission. Accessed 11/08/2016. [Online]. Available: <https://www.nasa.gov/planetarydefense/aida>
- [30] P. Michel, A. Cheng, M. Küppers, P. Pravec, J. Blum, M. Delbo, S. Green, P. Rosenblatt, K. Tsiganis, and J. Vincent, "Science case for the Asteroid Impact Mission (AIM): A component of the Asteroid Impact & Deflection Assessment (AIDA) mission," *Advances in Space Research*, vol. 57, no. 12, pp. 2529–2547, 2016.
- [31] H. Heidt, J. Puig-Suari, A. Moore, S. Nakasuka, and R. Twiggs, "Cubesat: A new generation of picosatellite for education and industry low-cost space experimentation," 2000.
- [32] AIM KUDOS Team, "RD2 AIM Mission and Payload Operations Scenario v0.9 Draft," European Space Research and Technology Centre, Tech. Rep., 2015.
- [33] R. Russel, "Radiative spin-up and spin-down of small asteroids," *Icarus*, no. 148, pp. 2–11, 2000.
- [34] P. Pravec and P. Scheirich, "Binary asteroid population: Secondary rotations and elongations," *Icarus*, vol. 267, pp. 267–295, 2016.
- [35] B. Chauvineau, P. Farinella, and F. Mignard, "Planar orbits about a triaxial body: Application to asteroidal satellites," *Icarus*, vol. 105, no. 2, pp. 370–384, 1993.
- [36] G. Balmino, "Gravitational potential harmonics from the shape of an homogeneous body," *Celestial Mechanics and Dynamical Astronomy*, vol. 60, no. 3, pp. 331–364, 1994.
- [37] K. Kumar, "Attitude dynamics and control of satellites orbiting rotating asteroids," *Acta Mechanica*, vol. 198, no. 1, pp. 99–118, 2008.
- [38] H. Hussmann, J. Oberst, K. Wickhusen, X. Shi, F. Damme, F. Lüdicke, V. Lupovka, and S. Bauer, "Stability and evolution of orbits around the binary asteroid 175706 (1996 FG3): Implications for the MarcoPolo-R mission," *Planetary and Space Science*, vol. 70, no. 1, pp. 102–113, 2012.
- [39] O. Montenbruck and E. Gill, *Satellite orbits: models, methods and applications*. Springer Science & Business Media, 2012.
- [40] T. Herring. (2013) Principles of the Global Positioning System Lecture Notes. Accessed 10/05/2016. [Online]. Available: <http://geoweb.mit.edu/~tah/12.540>
- [41] D. Richardson, O. Barnouin, L. Benner, W. Bottke, A. Campo Bagatin, A. Cheng, M. Hirabayashi, C. Maurel, J. McMahon, and P. Michel, "Dynamical and Physical Properties of 65803 Didymos," in *Lunar and Planetary Science Conference*, 2016.

- [42] F. Damme, H. Hussmann, E. Mai, J. Oberst, and K. Wickhusen, “Orbit stability in the Binary Asteroid System Didymos - An opportunity for spacecraft exploration,” 2015.
- [43] Jet Propulsion Laboratory. (2016) 65803 Didymos (1996GT). Accessed 01/03/2016. [Online]. Available: <http://ssd.jpl.nasa.gov/sbdb.cgi?sstr=65803+Didymos>
- [44] D. Rubincam, “Yarkovsky thermal drag on small asteroids and Mars-Earth delivery,” *Journal of Geophysical Research*, no. 103, pp. 1725–1732, 1998.
- [45] The Mathworks Inc. (2016) Modeling and simulation. Accessed 15/04/2016. [Online]. Available: <http://se.mathworks.com/discovery/modeling-and-simulation.html>
- [46] J. Wertz, *Spacecraft attitude determination and control*. Springer, 2012.
- [47] F. Markley and J. Crassidis, *Fundamentals of spacecraft attitude determination and control*. Springer, 2014.
- [48] B. Riwanto, “Cubesat attitude system calibration and testing,” Master’s thesis, Luleå University of Technology and Aalto University, Espoo, 2015.
- [49] D. Scheeres, S. J. Ostro, R. Hudson, E. DeJong, and S. Suzuki, “Dynamics of orbits close to asteroid 4179 Toutatis,” *Icarus*, vol. 132, no. 1, pp. 53–79, 1998.
- [50] G. Krasinsky and V. Brumberg, “Secular increase of astronomical unit from analysis of the major planet motions, and its interpretation,” *Celestial Mechanics and Dynamical Astronomy*, vol. 90, no. 3, pp. 267–288, 2004.
- [51] M. Sidi, *Spacecraft dynamics and control: a practical engineering approach*, ser. 10. UK: Cambridge University press, 1997.
- [52] D. J. Scheeres, “Orbital mechanics about small bodies,” 62nd International Astronautical Congress, 2011.
- [53] O. Montenbruck, E. Gill, and F. Lutze, *Satellite Orbits: Models, Methods and Applications*. Springer, 2002.
- [54] H. Schaub and J. Junkins, *Analytical mechanics of space systems*. AIAA, 2003.
- [55] N. Jovanović, “Aalto-2 satellite attitude control system,” Master’s thesis, Luleå University of Technology and Aalto University, Espoo, 2014.
- [56] D. Ilyas, *Orbital propagation and formation flying of cubesats QB50 within constellation*, 2011.
- [57] D. Vallado, *Fundamentals of astrodynamics and applications*. Springer Science & Business Media, 2001.

- [58] The Mathworks Inc. (2016) Aerospace toolbox functions. Accessed 15/04/2016.
- [59] P. Corke, *Robotics, vision and control: fundamental algorithms in MATLAB*. Springer, 2011.

A Quaternions

The kinematics of the satellite are expressed in quaternion form for computation purposes. This appendix contains the definition and the fundamental algebraic properties of this set of numbers. The sources of this information are [46, 55, 4]. A quaternion is a hyper complex number defined as

$$q = \hat{i}q_1 + \hat{j}q_2 + \hat{k}q_3 + q_4, \quad (\text{A1})$$

where \hat{i}, \hat{j} and \hat{k} are hyperimaginary numbers that satisfy the following conditions

$$\begin{aligned} \hat{i}^2 &= \hat{j}^2 = \hat{k}^2 = -1, \\ \hat{i}\hat{j} &= -\hat{j}\hat{i} = \hat{k}, \\ \hat{j}\hat{k} &= -\hat{k}\hat{j} = \hat{i}, \\ \hat{k}\hat{i} &= \hat{i}\hat{k} = \hat{j}. \end{aligned} \quad (\text{A2})$$

The parameter q_4 is the real or scalar part. Whereas the first three terms are denoted as the imaginary vector. When used for attitude representation, quaternions generally are defined as:

$$\begin{aligned} q_1 &= e_1 \sin\left(\frac{\theta}{2}\right), \\ q_2 &= e_2 \sin\left(\frac{\theta}{2}\right), \\ q_3 &= e_3 \sin\left(\frac{\theta}{2}\right), \\ q_4 &= \cos\left(\frac{\theta}{2}\right). \end{aligned} \quad (\text{A3})$$

Where $e_1 + e_2 + e_3 = 1$ which implies $\|q\| = 1$ and also that the use of these subset remains with constant length. Moreover, the fundamental mathematical operations of quaternions are addition, subtraction, multiplication, the norm and the inverse. The addition and subtraction obey the associative and commutative laws defined as

$$q_A \pm q_B = (q_{A1:3} \pm q_{B1:3}) + (q_{A4} \pm q_{B4}). \quad (\text{A4})$$

Addition and subtraction are done as normal vectors. The norm is also calculated the same way as in a vector or a complex number as

$$|q| = \sqrt{q_1^2 + q_2^2 + q_3^2 + q_4^2}. \quad (\text{A5})$$

The inverse is then

$$q^{-1} = \frac{q^*}{|q|}, \quad (\text{A6})$$

where q^* is the complex conjugate of q definded as

$$q = -\hat{i}q_1 - \hat{j}q_2 - \hat{k}q_3 + q_4 = (-q_{1:3} + q_4). \quad (\text{A7})$$

The multiplication of a quaternions is performed the same way as with complex numbers. However, it does not obey the commutative law, $q_A q_B \neq q_B q_A$. The next expression defines the multiplication:

$$q_C = q_A q_B = (\hat{i}q_{A1} + \hat{j}q_{A2} + \hat{k}q_{A3} + q_{A4}) (\hat{i}q_{B1} + \hat{j}q_{B2} + \hat{k}q_{B3} + q_{B4}). \quad (\text{A8})$$

In matrix form it becomes

$$\begin{bmatrix} q_{C1} \\ q_{C2} \\ q_{C3} \\ q_{C4} \end{bmatrix} = \begin{bmatrix} q_{B4} & q_{B3} & -q_{B2} & q_{B1} \\ -q_{B3} & q_{B4} & q_{B1} & q_{B2} \\ q_{B2} & -q_{B1} & q_{B4} & q_{B3} \\ -q_{B1} & -q_{B2} & -q_{B3} & q_{B4} \end{bmatrix} \begin{bmatrix} q_{A1} \\ q_{A2} \\ q_{A3} \\ q_{A4} \end{bmatrix}. \quad (\text{A9})$$

Given two successive rotations q_A and q_B , q_C becomes the quaternion that combines both rotations.

B Legendre Polynomials

The associated Legendre functions are defined as

$$P_{lm}(x) = (1 - x^2)^{m/2} \frac{d^m}{dx^m} (P_{l0}(x)). \quad (\text{B1})$$

The $P_{l0}(x)$ are the Legendre polynomials which are defined as

$$P_{l0} = \frac{1}{2^l l!} \frac{d^l}{dx^l} (x^2 - 1)^l \quad (\text{B2})$$

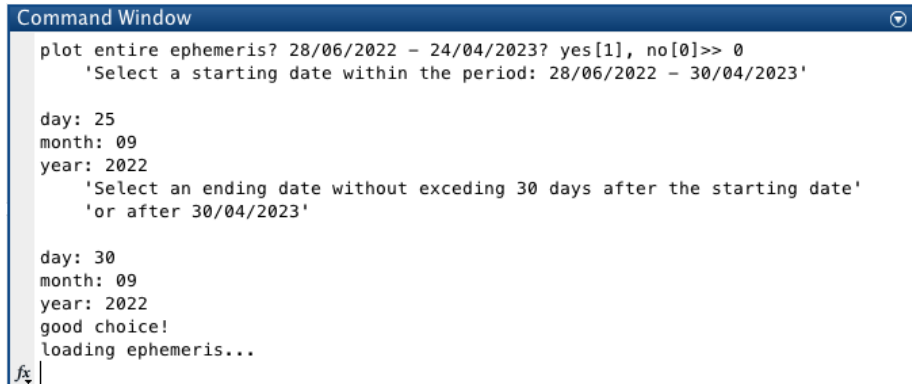
These functions and polynomials are used for the perturbation of a third body and in the spherical harmonic gravity field expansion. The list below contains the polynomials and functions up to degree and order 4. This information was taken from [1].

$$\begin{aligned} P_{00}(x) &= 1 \\ P_{10}(x) &= x \\ P_{11}(x) &= \sqrt{1 - x^2} \\ P_{20}(x) &= \frac{1}{2} (3x^2 - 1) \\ P_{21}(x) &= 3x\sqrt{1 - x^2} \\ P_{22}(x) &= 3(1 - x^2) \\ P_{30}(x) &= \frac{1}{2} (5x^3 - 3x) \\ P_{31}(x) &= \frac{3}{2} (5x^2 - 1) \sqrt{1 - x^2} \\ P_{32}(x) &= 15x(1 - x^2) \\ P_{33}(x) &= 15(1 - x^2)\sqrt{1 - x^2} \\ P_{40}(x) &= \frac{1}{8} (35x^4 - 30x^2 + 3) \\ P_{41}(x) &= \frac{5}{2} (7x^3 - 3x) \sqrt{1 - x^2} \\ P_{42}(x) &= \frac{15}{2} (7x^2 - 1)(1 - x^2) \\ P_{43}(x) &= 105x(1 - x^2)\sqrt{1 - x^2} \\ P_{44}(x) &= 105(1 - x^2)^2 \end{aligned} \quad (\text{B3})$$

C Simulation set-up

An initial set-up of the simulator must be done before computing the environment disturbances. This set-up consists of loading the data corresponding to a specific time period of the ephemeris of the Didymos asteroid and the configuration of the satellite parameters, the orbit propagator, the Didymos system properties and the environment disturbances parameters.

The first step consists of extracting the information of the Didymos ephemeris. One must choose a time between the 28th June of 2022 and the 24th April of 2023, which corresponds to the period of the mission. The chosen period cannot exceed 5 days because Matlab cannot handle a larger variable than this. The timescale is sufficient for the ADCS design. Figure C1 shows the interface when selecting the dates of interest.



```
Command Window
plot entire ephemeris? 28/06/2022 - 24/04/2023? yes[1], no[0]>> 0
'Select a starting date within the period: 28/06/2022 - 30/04/2023'

day: 25
month: 09
year: 2022
>Select an ending date without exceeding 30 days after the starting date'
'or after 30/04/2023'

day: 30
month: 09
year: 2022
good choice!
loading ephemeris...
f|
```

Figure C1: Selecting the dates of interest to load the ephemeris of the Didymos.

Another feature of the simulator is the possibility to plot the trajectory of the asteroid and the Earth in the Heliocentric reference frame. This is done after loading the ephemeris into the workspace of Matlab. One can decide to choose the trajectory of the whole mission or just a partial trajectory according to the period of time chosen. Figure C2 and Figure C3 shows both cases respectively.

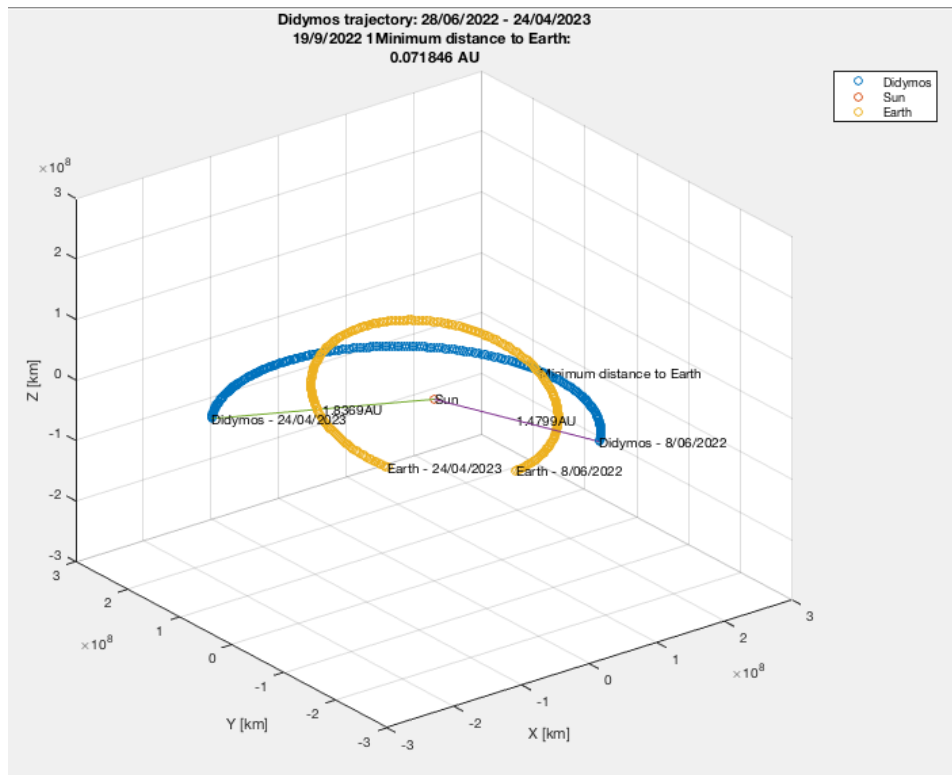


Figure C2: Trajectory of the Didymos asteroid corresponding to the expected complete period of the mission: 28/06/2022 - 24/04/2023.

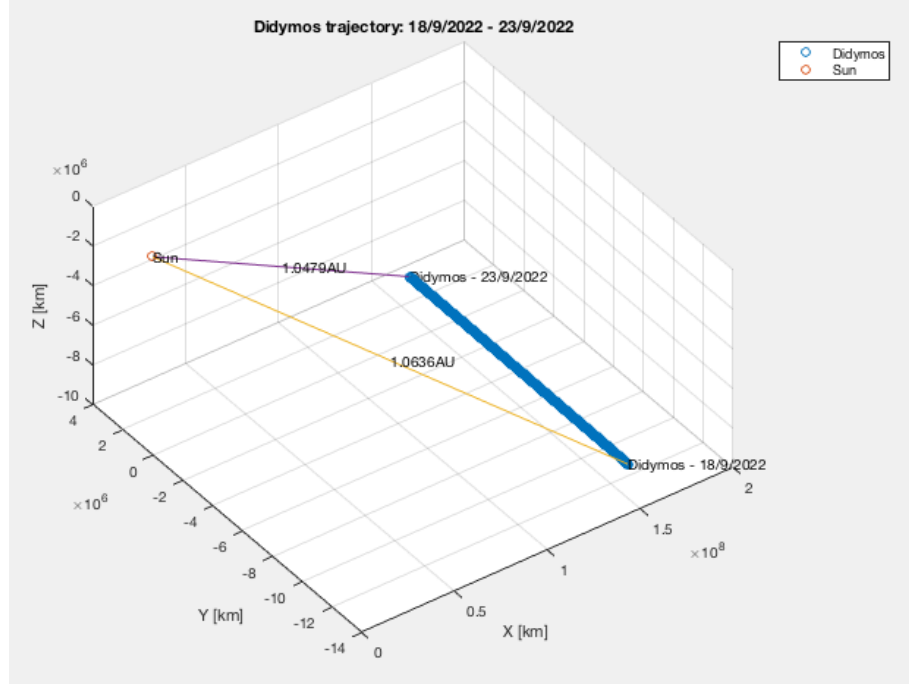


Figure C3: Example of a partial trajectory of the Didymos asteroid between the dates 19/09/2022 - 23/09/2022.

The following step is to open the Simulink model (shown in Figure C4) and adjusting the parameters corresponding to the satellite (Figure C5a), the didymos system (Figure C5b), the orbit (Figure C5c) and the environment disturbances (Figure C5d). The list of the adjustable parameters is also given in Section 6.

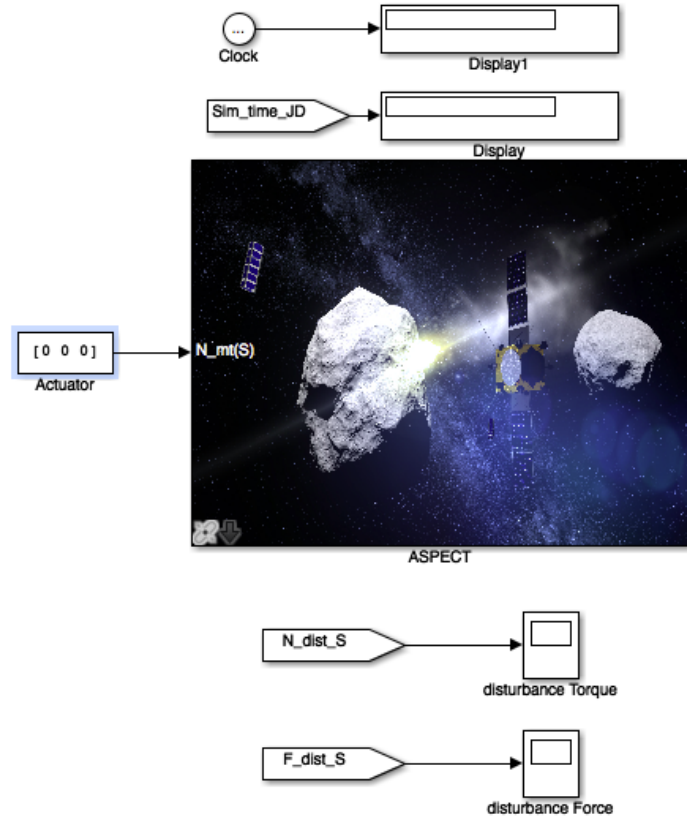


Figure C4: SIMULINK model of the disturbances. Image corresponding to the principal layer of the simulator.

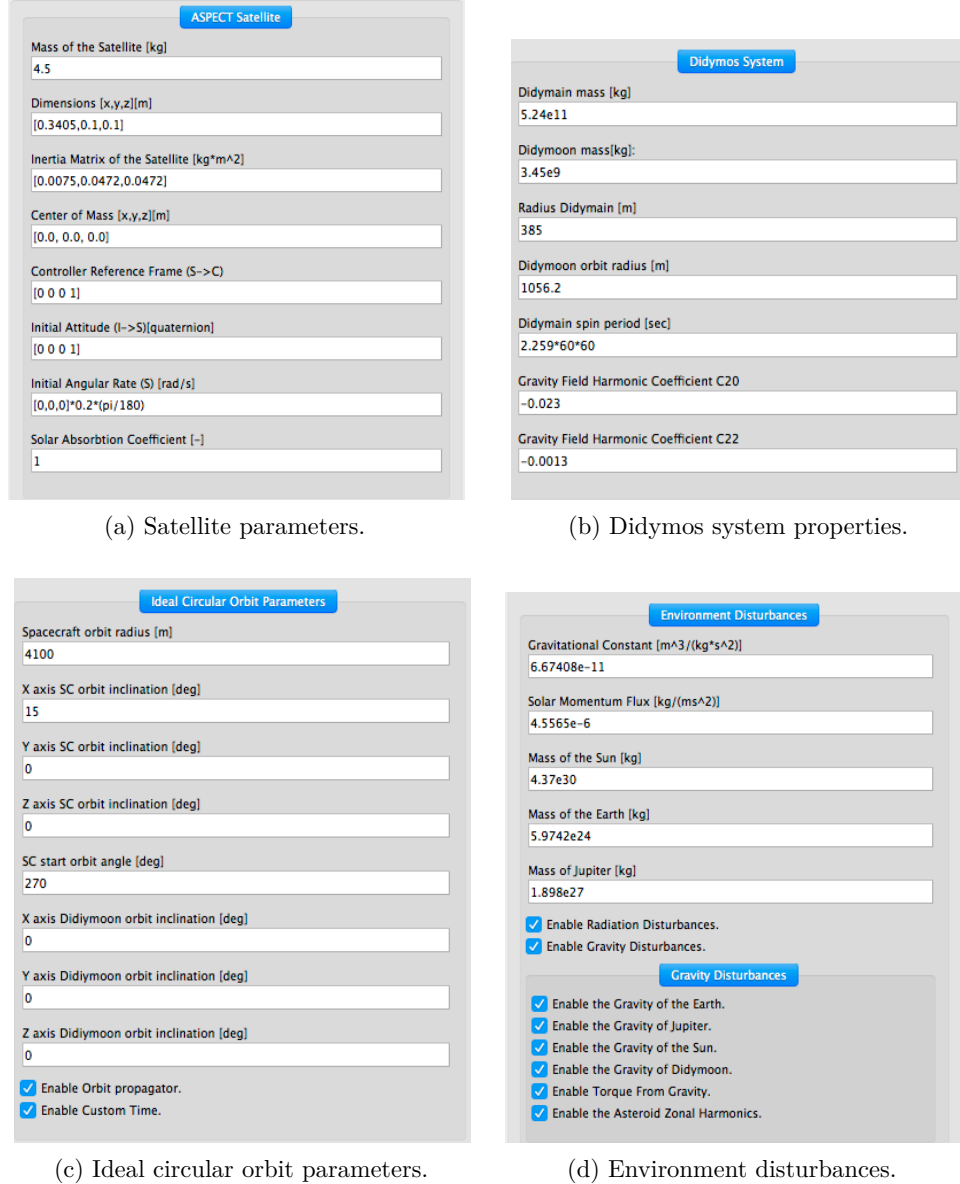


Figure C5: SIMULINK model masks containing the adjustable parameters of the simulation.

Finally, all the initial and final variables handled during the simulation are stored in the Matlab workspace. The data comes in different types of variables such as constants, matrices or timeseries. These can be later manipulated as desired in order to perform the disturbance or the ADCS analysis. Figure C6 depicts a portion of the workspace containing the variables of interest.

Name	Value
average_didymoon_torque	7.9220e-12
average_didymos_torque	1.0931e-09
average_distance_didymos	1.0117
average_earth_torque	6.4281e-19
average_jupiter_torque	2.4023e-20
average_line	1x1 Line
average_srp_torque	2.4926e-08
average_sun_torque	3.5009e-15
average_zharm_torque	3.8950e-13
d_end	'1.0111'
d_ini	'1.0123'
da	19
date_graph	'2022-10-10'
date_graph_end	'11/10/2022'
date_graph_start	'10/10/2022'
didymoon_l	1x1 double times...
didymos	1441x4 global d...
didymos2	301x4 double
didymos_sim	1x1 double times...
dis_e_d	301x3 double
earth	1x1 double times...
earth1	1x1 double times...
earth_pos_total	301x3 double
end_day	11
end_month	10
end_year	2022
force_didymoon	1x1 double times...
force_didymos	1x1 double times...
force_earth	1x1 double times...
force_jupiter	1x1 double times...
force_srp	1x1 double times...
force_sun	1x1 double times...
force_zharm	1x1 double times...

Figure C6: Output variables in the workspace of the Matlab environment.